nature nanotechnology

ARTICLES

https://doi.org/10.1038/s41565-020-00781-4

Check for updates

A general strategy towards personalized nanovaccines based on fluoropolymers for post-surgical cancer immunotherapy

Jun Xu[1], Jia Lv[2], Qi Zhuang[1], Zongjin Yang[1], Zhiqin Cao[1], Ligeng Xu[1], Pei Pei[3], Chenya Wang[1], Hanfei Wu[1], Ziliang Dong[1], Yu Chao[1], Chao Wang[1], Kai Yang[3], Rui Peng[1]✉, Yiyun Cheng[4,2]✉ and Zhuang Liu[1]✉

Cancer metastases and recurrence after surgical resection remain an important cause of treatment failure. Here we demonstrate a general strategy to fabricate personalized nanovaccines based on a cationic fluoropolymer for post-surgical cancer immunotherapy. Nanoparticles formed by mixing the fluoropolymer with a model antigen ovalbumin, induce dendritic cell maturation via the Toll-like receptor 4 (TLR4)-mediated signalling pathway, and promote antigen transportation into the cytosol of dendritic cells, which leads to an effective antigen cross-presentation. Such a nanovaccine inhibits established ovalbumin-expressing B16-OVA melanoma. More importantly, a mix of the fluoropolymer with cell membranes from resected autologous primary tumours synergizes with checkpoint blockade therapy to inhibit post-surgical tumour recurrence and metastases in two subcutaneous tumour models and an orthotopic breast cancer tumour. Furthermore, in the orthotopic tumour model, we observed a strong immune memory against tumour rechallenge. Our work offers a simple and general strategy for the preparation of personalized cancer vaccines to prevent post-operative cancer recurrence and metastasis.

Cancer immunotherapy has brought great hope to the fight against cancer in recent years[1,2]. Different types of cancer immunotherapy strategies, have been extensively studied or tested in the clinic[3], alone or in combination with other conventional therapeutic strategies, such as chemotherapy[4,5] or radiotherapy[6,7]. Moreover, it has been reported that post-surgery immunotherapy, such as immune checkpoint blockade (ICB) therapy, may be able to reduce the risk of cancer recurrence and metastasis[8,9]. However, its therapeutic benefits remain to be improved.

Among various types of cancer immunotherapy, cancer vaccines can induce tumour-specific immune responses[10–12]. To activate and expand tumour-specific T cells, recent advances in nanoparticle (NP)-based vaccines (nanovaccines) have focused on the co-delivery of tumour-specific antigens and adjuvants to antigen-presenting cells (APCs), such as dendritic cells (DCs)[13–15]. In this process, cytosolic delivery and cross-presentation of antigens by professional DCs via the major histocompatibility complex class I (MHC-I) antigen-presenting pathway are essential to trigger robust antitumour responses[16,17]. Therefore, to fabricate efficient cancer nanovaccines, it is critical to develop antigen carriers that act as immune adjuvants, and are capable of shuttling antigens directly into the cytosol of APCs.

Recently, fluoropolymers, such as fluorinated dendrimers and polyethyleneimines (PEIs), were reported to be promising gene and protein delivery carriers[18–20]. Fluorocarbon chains grafted on these cationic polymers could enhance their abilities to mediate the transmembrane delivery of cargoes into the cell cytosol, owing to the low surface energy and lipophobicity of fluoroalkyl chains[21,22]. Here we hypothesized that such fluoropolymers might also be employed as antigen carriers to fabricate tumour nanovaccines with an efficient antigen cross-presentation. We found that two types of fluoroalkane-grafted polyethyleneimines (F-PEIs), F_7-PEI and F_{13}-PEI, both showed reduced cytotoxicity compared with that of bare PEI, and, when mixed with a model protein antigen ovalbumin (OVA), would self-assemble to form F-PEI/OVA NPs. Such F-PEI/OVA NPs, especially the formulation with higher fluorine content, could promote high levels of antigen cross-presentation due to the efficient cytosolic delivery of OVA. In vivo, such a formulation elicits high levels of antitumour T-cell responses, which leads to an effective inhibition of established B16-OVA tumours. We further demonstrate that the fluoropolymer could be employed to fabricate personalized cancer vaccines by mixing it with tumour cell membranes collected from the surgically resected autologous tumours. Such fluoropolymer-based personalized nanovaccines, when combined with ICB, are able to prevent post-operative tumour recurrence and tumour metastases, as shown in two subcutaneous tumour models and an orthotopic breast cancer tumour. Our work presents a simple and reliable strategy to fabricate cancer nanovaccines based on fluoropolymers, promising for an effective patient-specific post-surgery immunotherapy.

Fluoropolymer for antigen delivery

F-PEIs were synthesized via an amine–epoxide reaction (Fig. 1a)[20] to obtain F_7-PEI and F_{13}-PEI. The average number of

[1]Institute of Functional Nano & Soft Materials (FUNSOM), Jiangsu Key Laboratory for Carbon-Based Functional Materials and Devices, Soochow University, Suzhou, China. [2]South China Advanced Institute for Soft Matter Science and Technology, South China University of Technology, Guangzhou, China. [3]State Key Laboratory of Radiation Medicine and Protection, School of Radiation Medicine and Protection and School for Radiological and Interdisciplinary Sciences (RAD-X), Collaborative Innovation Center of Radiation Medicine of Jiangsu Higher Education Institutions, Soochow University, Suzhou, China. [4]Shanghai Key Laboratory of Regulatory Biology, School of Life Sciences, East China Normal University, Shanghai, China. ✉e-mail: rpeng@suda.edu.cn; yycheng@mail.ustc.edu.cn; zliu@suda.edu.cn

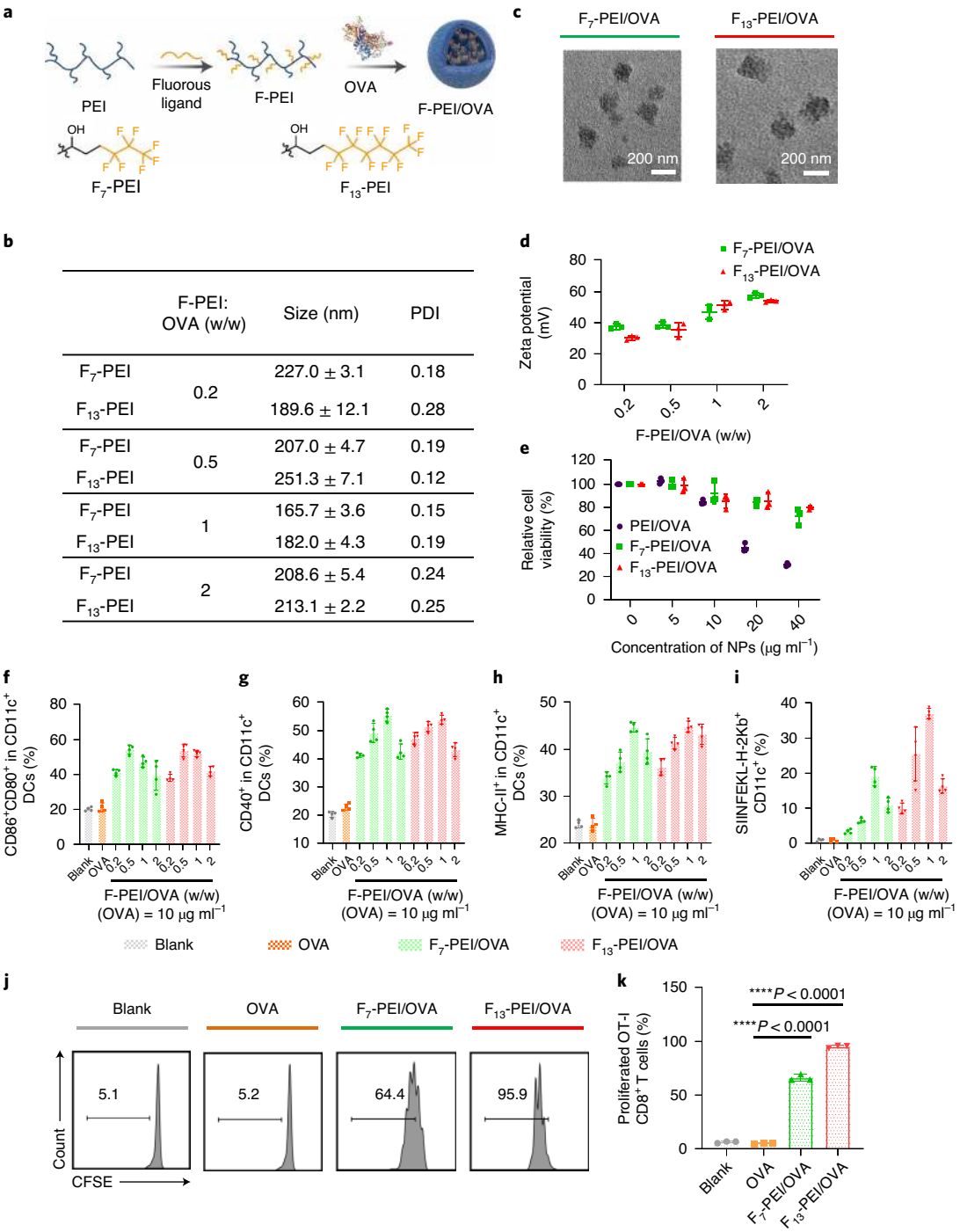

	F-PEI: OVA (w/w)	Size (nm)	PDI
F_7-PEI	0.2	227.0 ± 3.1	0.18
F_{13}-PEI		189.6 ± 12.1	0.28
F_7-PEI	0.5	207.0 ± 4.7	0.19
F_{13}-PEI		251.3 ± 7.1	0.12
F_7-PEI	1	165.7 ± 3.6	0.15
F_{13}-PEI		182.0 ± 4.3	0.19
F_7-PEI	2	208.6 ± 5.4	0.24
F_{13}-PEI		213.1 ± 2.2	0.25

Fig. 1 | Preparation, characterization and DC activation of nanovaccines. a, Schematic illustration to show the preparation of F-PEI/OVA nanovaccines. **b**, Hydrodynamic sizes of F_7-PEI/OVA and F_{13}-PEI/OVA NPs prepared at varied polymer/OVA ratios (w/w), as measured by dynamic light scattering. **c**, Transmission electron microscopy images of the F_7-PEI/OVA (left) and F_{13}-PEI/OVA (right) NPs (F-PEI:OVA = 1:1 w/w). Representative images from three independent experiments are shown. **d**, Zeta potentials of the F_7-PEI/OVA and F_{13}-PEI/OVA NPs. **e**, Relative viabilities of BMDCs after incubation with increasing OVA concentrations of PEI/OVA, F_7-PEI/OVA or F_{13}-PEI/OVA NPs for 24 h. **d**,**e**, $n = 3$ independent experiments using the same batch of F_7-PEI and F_{13}-PEI. **f**–**i**, Statistical data showing $CD86^+CD80^+$ (**f**), $CD40^+$ (**g**), MHC-II^+ BMDC (**h**) and OVA antigen cross-presentation (**i**) efficiencies in BMDCs treated with OVA, F_7-PEI/OVA or F_{13}-PEI/OVA NPs at the indicated F-PEI:OVA ratios for 12 h ($n = 4$ independent replicates). The OVA concentration was fixed at 10 μg ml^{-1}. **j**,**k**, Representative flow cytometry plots (**j**) and the statistical data (**k**) showing proliferating (carboxyfluorescein succinimidyl ester (CFSE) dilution) of OT-I $CD3^+CD8^+$ T cells after incubation with BMDCs pulsed with OVA, F_7-PEI/OVA or F_{13}-PEI/OVA NPs at the F-PEI:OVA ratio of 1:1 ($n = 3$ independent replicates). **d**–**i**,**k**, Data presented as mean ± standard deviation (s.d.). **f**–**i**,**k**, Representative data from at least three independent experiments with similar results. **k**, Statistical significance between the indicated groups was determined using two-sided unpaired *t*-tests. ****$P < 0.0001$. PDI, polydispersity index.

3-(perfluoro-*n*-hexyl)-1,2-propenoxide ligands conjugated per PEI was determined to be ~30 in F_{13}-PEI (fluorine content = 20.49%), whereas the average number of 3-(perfluoro-*n*-propyl)-1,2-propenoxide ligands conjugated per PEI was ~27 in F_7-PEI (fluorine content = 12.02%) (Supplementary Fig. 1). The obtained F_7-PEI and F_{13}-PEI were mixed with OVA at different weight ratios (w/w, pH 7.0) (Fig. 1b). The formed NPs showed hydrodynamic sizes in the range of 157–250 nm (Fig. 1b,c) and similar zeta potentials at around +50 mV (Fig. 1d). As the control sample, intact branched PEI (25 kDa) was also able to prepare NPs on mixing with OVA, and the obtained PEI/OVA NPs showed sizes and surface charges comparable to those of F-PEI/OVA NPs (Supplementary Fig. 2a,b).

We then studied the interactions of our F-PEI/OVA NPs with mouse bone marrow-derived dendritic cells (BMDCs). First, our tested samples had rather low levels of endotoxin (Supplementary Table 1) and F-PEI/OVA NPs showed no striking cytotoxicity to BMDCs in our tested concentration range, in contrast to PEI/OVA NPs prepared with non-modified PEI, which appeared to be highly toxic (Fig. 1e and Supplementary Fig. 3). Such a high cytotoxicity of unmodified PEI excluded the possibility of using PEI/OVA for further DC activation experiments.

The maturation of DCs is critical for antigen presentation and the initiation of subsequent immune responses[23–26]. Interestingly, BMDCs pulsed with either F_{13}-PEI/OVA or F_7-PEI/OVA at the F-PEI:OVA ratio of 1:1 showed the highest upregulation in co-stimulatory molecules (CD80, CD86, CD40 and MHC-II) compared with those treated with F-PEI/OVA at other ratios (Fig. 1f–h and Supplementary Fig. 4a). Consistent with DC maturation data, F_{13}-PEI/OVA and F_7-PEI/OVA (F-PEI:OVA = 1:1 w/w) induced the highest production of tumour necrosis factor-α (TNF-α), interleukin-6 (IL-6) and IL-12p70 (Supplementary Fig. 4b–d) by treated BMDCs.

We then examined the cross-presentation efficiency for DCs treated with F-PEI/OVA NPs. Treating BMDCs by F_{13}-PEI/OVA NPs (F_{13}-PEI:OVA = 1:1 w/w) resulted in the highest level of the SIINFEKL peptide presented on the BMDCs' surface (Fig. 1i and Supplementary Fig. 5a,b). We hypothesized that at the higher F-PEI:OVA ratios, such as 2:1 and above, the fluoropolymer would have a stronger binding with the antigen, and thus hinder its release for further antigen cross-presentation. Together, our data suggest that both F_{13}-PEI/OVA and F_7-PEI/OVA at the optimal F-PEI:OVA ratio of 1:1 could trigger an efficient DC maturation, but the former, F_{13}-PEI/OVA, appeared to be more effective in inducing antigen cross-presentation.

Using an in vitro OT-I $CD8^+$ T-cell priming assay, BMDCs pre-treated with F_{13}-PEI/OVA NPs could induce a significant proliferation of OT-I $CD8^+$ T cells to a level much higher than those induced by BMDCs pre-treated with OVA or F_7-PEI/OVA (Fig. 1j,k). Meanwhile, greatly increased secretions of TNF-α and interferon-γ (IFN-γ) (Supplementary Fig. 6) were also observed for those $CD8^+$ T cells activated by F_{13}-PEI/OVA-pre-treated BMDCs. These data suggest that F_{13}-PEI/OVA could effectively activate BMDCs and trigger subsequent OVA-specific T-cell responses.

The underlying mechanisms of such fluoropolymer-based NPs to promote cross-presentation and DC maturation were subsequently studied. The model antigen OVA was labelled with fluorescein isothiocyanate (FITC) to facilitate intracellular tracking. Both F_{13}-PEI/OVA-FITC NPs and F_7-PEI/OVA-FITC NPs showed a greatly enhanced uptake by BMDCs compared with that of OVA-FITC alone (Fig. 2a).

A recent study demonstrated that PEI could re-polarize myeloid-derived suppressor cells (MDSCs) from M2- to M1-type through the Toll-like receptor 4 (TLR4)-mediated signalling pathway[27]. Interestingly, the cellular uptakes of F_7-PEI/OVA-FITC and F_{13}-PEI/OVA-FITC NPs by BMDCs from *Tlr4* gene knockout mice ($Tlr4^{-/-}$) were found to be significantly lower than that by BMDCs from wild-type (wt) mice (C57BL/6), which suggests the possible involvement of TLR4-dependent endocytosis in the internalization of F-PEI-based NPs (Fig. 2b). In addition, $Tlr4^{-/-}$ BMDCs appeared to be much more inert to treatments with F_7-PEI, F_{13}-PEI, F_7-PEI/OVA, F_{13}-PEI/OVA or a classical TLR4 agonist lipopolysaccharide (LPS), which indicates that F-PEI and F-PEI/OVA may possibly activate DCs via the TLR4 signalling pathway (Fig. 2c). Using murine TLR4 (NF-κB-SEAP/KI-[IL-8]Lucia) dual-reporter HEK293 cells with a stable transfection of mouse TLR4 (mTLR4) MD-2/CD14 genes, we further confirmed that our fluoropolymers and fluoropolymer-based NPs could, indeed, trigger TLR4 activation in a dose-dependent manner, especially when carrying OVA (Fig. 2d and Supplementary Fig. 7). Additional experiments further indicated that, beyond activating TLR4, the DC maturation triggered by F-PEI/OVA NPs may also be related to other pathways, such as the inflammasome signalling pathway (Supplementary Fig. 8a)[28].

Besides the TLR4-dependent endocytosis, we also investigated other endocytosis pathways for these fluoropolymer-based NPs by using dynasore, a dynamin inhibitor of clathrin-mediated endocytosis, or genistein, an inhibitor of caveolae-dependent endocytosis, and uncovered that both pathways should be involved in the internalization of these F-PEI-based NPs (Supplementary Fig. 9). Meanwhile, most of the OVA-FITCs delivered by F-PEI were not co-localized with lysosomes and instead evenly distributed within cells after 4–6 h, which indicates an efficient endosomal escape of the protein antigen delivered by our fluoropolymers (Fig. 2e, Supplementary Fig. 10). In contrast, the intracellular protein delivery by bare PEI appeared to be much less efficient. Furthermore, the F-PEI/OVA NPs after cell entry would dissociate to release the protein antigen, a behaviour favourable for antigen presentation by DCs (Supplementary Fig. 11).

The intracellular delivery of OVA-FITC by fluoropolymers F_7-PEI and F_{13}-PEI in the presence of bafilomycin A1, which prevents the acidification of endosomes[29], was also studied. We observed trapped F-PEI/OVA NPs in endosomes and/or lysosomes, which suggests that the pH buffering mechanism would, indeed, occur during the endosomal escape of F-PEI-based NPs (Supplementary Fig. 12). Notably, besides the pH buffering effect attributed to the PEI backbone, the fluoroalkyl chains may also play a unique role here in enhancing the cellular uptake and endosomal escape of F-PEI/OVA NPs. With hydrophobic and lipophobic characteristics, such fluoroalkyl chains would be easily fused with membrane lipids via hydrophobic interactions, and their lipophobic characteristic could ensure a rapid diffusion of the fluoroalkyl chains across the lipid membranes[20,30].

Fluoropolymer-based nanovaccines exhibit robust immune responses in vivo

In vivo experiments were next carried out to evaluate the immunization efficacy of F-PEI/OVA nanovaccines (Fig. 3a). The fluoropolymer-based NPs were similarly able to enhance the antigen uptake by DCs in the immunized mice (Supplementary Fig. 13). Consistent with in vitro results, vaccination with F_{13}-PEI/OVA triggered the highest level of $CD86^+CD80^+$ BMDCs in the inguinal lymph nodes (LNs) of treated mice compared with that induced by OVA alone or F_7-PEI/OVA treatment on day 3 after immunization (Fig. 3b–d and Supplementary Fig. 14). Notably, F_{13}-PEI/OVA also resulted in the highest level of $CD11c^+$SIINFEKL-H-$2Kb^+$ antigen cross-presented DCs in draining LNs five-day post-immunization (Fig. 3e). Furthermore, F_7-PEI and F_{13}-PEI could elicit Th1-polarized immune responses, as shown by an OVA-specific immunoglobulin $(IgG)_{2a}/IgG_1$ ratio of >1 (Fig. 3f), and the F_{13}-PEI/OVA nanovaccine could induce an effective production of IFN-γ (Fig. 3g).

F-PEI/OVA-induced OVA-specific T-cell immune responses were then investigated on day 7 (Fig. 3b). Notably, the frequency

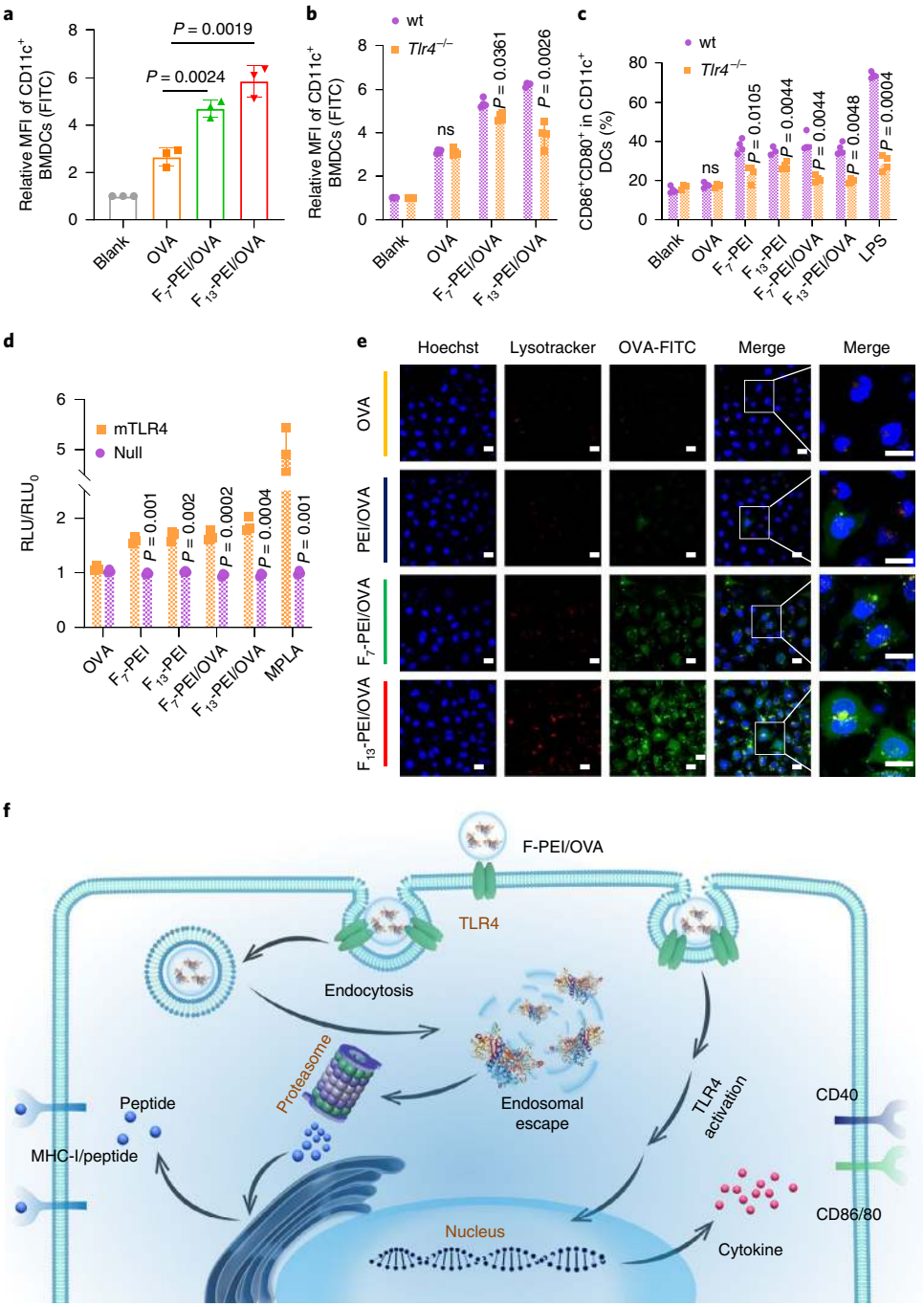

Fig. 2 | In vitro DC activation by nanovaccines. a,**b**, Cell-uptake analysis of nanovaccines. The extracellular fluorescence was quenched by trypan before the flow cytometry assay. **a**, Flow cytometry measurement of the mean fluorescence intensity (MFI) of $CD11c^+$ cells after incubation with FITC-OVA, F_7-PEI/FITC-OVA or F_{13}-PEI/FITC-OVA for 12 h. **b**, Flow cytometry measurement of MFI for wt or *Tlr4*$^{-/-}$ BMDCs incubated with F_7-PEI/FITC-OVA or F_{13}-PEI/FITC-OVA. **c**, Maturation levels of BMDCs collected from wt mice and *Tlr4*$^{-/-}$ mice after being treated with the indicated samples. Free OVA and LPS were used as the negative and positive controls, respectively. **d**, HEK-Dual Null (NF/IL8) cells (as control) and HEK-Dual mTLR4 (NF/IL-8) cells were stimulated with 10 μg ml^{-1} OVA, F_7-PEI, F_{13}-PEI, F_7-PEI/OVA or F_{13}-PEI/OVA. The TLR4 agonist MPLA (1 μg ml^{-1}) was used as the positive control. After 12 h of incubation, activation of the promoter via TLR4 was determined by measuring the Lucia luciferase activity using QUANTI-Luc, a Lucia luciferase detection reagent. RLU, relative light unit of treated groups; RLU_0, RLU of the blank. **a**–**d**, Data presented as mean ± s.d. **a**,**d**, $n = 3$ independent experiments using the same F_7-PEI or F_{13}-PEI. **b**,**c**, $n = 4$ independent experiments using the same F_7-PEI or F_{13}-PEI. Statistical significance between the indicated groups was determined using two-sided unpaired *t*-tests. **e**, Confocal fluorescence images of DC2.4 cells treated with OVA-FITC (green), PEI/OVA-FITC (green), F_7-PEI/OVA-FITC (green) or F_{13}-PEI/OVA-FITC (green) for 6 h. The nuclei and acidic compartments (endosomes and lysosomes) were stained with Hoechst (blue) and LysoTracker (red), respectively. Representative images from three independent experiments are shown. Scale bar, 10 μm. **f**, A scheme showing the mechanism of F-PEI/OVA NPs to enhance the intracellular uptake of OVA, promote antigen cross-presentation and activate DCs via a TLR4-mediated manner.

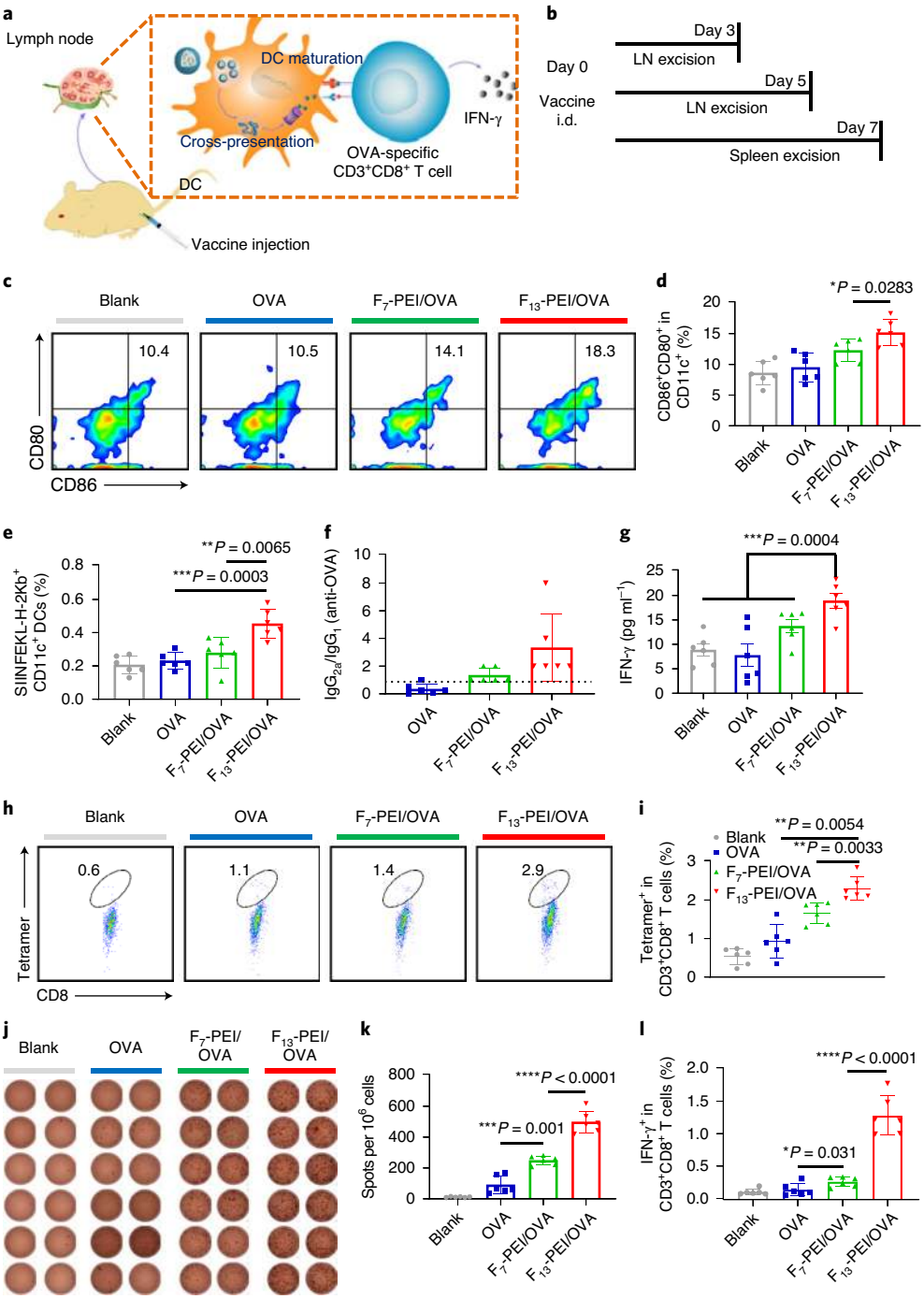

Fig. 3 | In vivo immune stimulation by F-PEI/OVA nanovaccines. a,**b**, Scheme (**a**) and timeline (**b**) of the experimental design to evaluate the in vivo immune responses triggered by F-PEI/OVA nanovaccines. **c**,**d**, Representative flow cytometry data (**c**) and statistical data (**d**) to show DC maturation induced by different formulations of NPs in vivo on day 3 post-immunization. **e**, Proportions of $CD11c^+SIINFEKL^+$ SIINFEKL-presenting DCs in the LNs on day 5 post-immunization. **f**,**g**, Ratios of OVA-specific IgG_{2a}:IgG_1 (**f**) and IFN-γ production (**g**) in sera of immunized mice on day 7 post-immunization. **h**,**i**, Representative flow dot plots (**h**) and statistical data (**i**) of the H-2Kb/SIINFEKL tetramer staining of $CD3^+CD8^+$ T cells in the spleen on day 7 post-immunization. **j**,**k**, IFN-γ spot-forming cells (SFCs) (**j**) and statistical data (**k**) from restimulated splenocytes determined by the ELISPOT assay on day 7 post-immunization. **l**, The percentages of IFN-γ-positive cells in $CD8^+$ T cells from restimulated splenocytes on day 7 post-immunization. **d**–**g**,**i**,**k**,**l**, Data presented as mean ± s.d. ($n = 6$ biologically independent mice for each group). **d**,**e**,**i**,**k**,**l**, Statistical significance between the indicated groups was determined using two-sided unpaired *t*-tests. Statistical significance in **g** was calculated by one-way analysis of variance. $^*P < 0.05$, $^{**}P < 0.01$, $^{***}P < 0.001$, $^{****}P < 0.0001$. i.d., intradermal.

of SIINFEKL-MHC-I tetramer$^+$CD8$^+$ T cells presented a sixfold increase in the F_{13}-PEI/OVA NP group compared with that in the OVA group, and a twofold increase compared with that in the F_7-PEI/OVA group (Fig. 3h,i and Supplementary Fig. 15). Typically, stronger antigen-specific T-cell mediated immune responses occur on the second exposure to the same antigen[31]. During this process,

T cells rapidly eliminate any cells that express this surface antigen by secreting IFN-γ. On the second exposure to the same antigen, OVA peptide (SIINFEKL), IFN-γ ELISPOT (enzyme-linked immune absorbent spot) responses (Fig. 3j,k) and the relative ratios of IFN-γ$^+$CD8$^+$ T cells (Fig. 3l and Supplementary Fig. 16) in the splenocytes from the mice immunized with F_{13}-PEI/OVA were both found to be significantly increased, which demonstrates the robust in vivo antigen-specific T-cell immune responses triggered by the F_{13}-PEI/OVA nanovaccine. Notably, the adaptive T-cell responses triggered by F_{13}-PEI/OVA appeared to be much lower in *Tlr4*$^{-/-}$ mice (Supplementary Fig. 17), which further demonstrates the TLR4-mediated immune activation pathway for our F-PEI-based nanovaccine.

To further assess the immune protection effect induced by the F-PEI/OVA nanovaccines, immunized mice were challenged with OVA-expressing B16-OVA melanoma tumour cells seven days post the final immunization (Fig. 4a). For mice injected with F_{13}-PEI/OVA NPs, their average tumour volume was considerably smaller than that in the other groups at all time points (Fig. 4b), and their survivals were significantly prolonged (Fig. 4c). Consistent with our previous observation (Fig. 3j,k), ELISPOT responses and the relative ratios of IFN-γ$^+$CD8$^+$ T cells (Supplementary Fig. 18) in the splenocytes of F_{13}-PEI/OVA-immunized mice collected on day 21 were found to be the highest among all the tested groups.

The therapeutic effect of the F-PEI-based nanovaccines was also evaluated using the B16-OVA melanoma tumour model. CpG oligonucleotide, a TLR-9 agonist, and aluminium (alum) were both chosen as the control adjuvant. In the PBS and OVA control groups, all the animals died within 25 days. The OVA + CpG, OVA + alum and F_7-PEI/OVA groups conferred a minor degree of immune therapeutic effect. In contrast, F_{13}-PEI/OVA-immunized mice maintained an evidently high survival rate, with 37.5% up to 60 days (Fig. 4d–g), which demonstrates the potential of F_{13}-PEI/OVA as a therapeutic cancer vaccine.

To facilitate in vivo tracking, F-PEI/OVA NPs were radiolabelled with ^{125}I (labelling on OVA) and injected at the tail base of mice for biodistribution studies at different time points. Significant retention of the nanovaccines was observed in the draining LN (Supplementary Fig. 19). Major organs, which included the liver, spleen, kidney, heart and lung, were collected and sliced for haematoxylin and eosin staining. No obvious sign of organ damage or inflammatory lesion was observed for mice seven days after the intradermal injection with F_{13}-PEI/OVA three times (Supplementary Fig. 20), which suggests that F_{13}-PEI/OVA NPs may be used as a safe and effective nanovaccine.

Fluoropolymer-based personalized nanovaccine for treating post-surgical distant tumours

Residual microtumours or circulating tumour cells may cause lethal tumour recurrence and metastasis months or even years post-operation. Cancer vaccines developed from lysates of surgically collected tumour cells represent a promising avenue for cancer immunotherapy[32–34]. We carried out a more clinically relevant study by using the cancer cell membrane collected from resected tumours as the source of tumour antigens and F_{13}-PEI as the antigen carrier (F_{13}-PEI/Mem) to fabricate the F_{13}-PEI-based nanovaccine, which was then used together with ICB therapies to treat leftover tumours post-surgery (Fig. 5a).

By simply mixing collected Mem with F_{13}-PEI, positively charged F_{13}-PEI/Mem NPs with an average size of ~50 nm could be easily obtained (Supplementary Fig. 21). Here, in our experiments, each C57BL/6 mouse was subcutaneously inoculated with two B16F10 melanoma tumours on both right and left flanks. Next, each mouse after surgical resection of its tumour on one side was intradermally injected at the site of the tail base with F-PEI-based vaccines that contained tumour cell membranes collected from the same mouse (Fig. 5a,b). The tumour growth on the opposite side of each mouse was then closely monitored (Fig. 5c and Supplementary Fig. 22). Notably, the tumour growth on the mice immunized with F_{13}-PEI/Mem was significantly delayed, compared that on unimmunized mice and mice immunized with Mem alone. Anti-PD1 (programmed cell death protein 1) therapy could further promote the antitumour efficacy of F_{13}-PEI/Mem. The therapeutic response of F_{13}-PEI/Mem + anti-PD1 appeared to be much better than that achieved by anti-PD1 alone or by Mem + anti-PD1. In fact, after the treatment with F_{13}-PEI/Mem + anti-PD1, 4 of the 6 mice became tumour free and survived for over 60 days (Fig. 5d), which demonstrates the therapeutic benefit of such combination therapy.

In addition to the B16F10 melanoma tumour, we then tested our strategy to treat CT26 murine colon tumours, which display a partial response to anti-CTLA4 blockade in preclinical experiments[35]. Similar to the results in treating B16F10 tumours, F_{13}-PEI/Mem NPs + anti-CTLA4 treatment resulted in the most significant tumour growth suppression and 50% of those mice survived up to 60 days, much better than the therapeutic responses achieved in other control groups (Fig. 5e–g). The body weights of mice were not impacted by the treatment (Supplementary Fig. 23).

Next, we sought to verify that the observed antitumour immune responses triggered by such membrane-based nanovaccines were, indeed, related to the tumour-specific neoantigens expressed on the tumour cell membrane. The murine CT26 colon carcinoma model was recently reported to harbour a single-point mutation within the Slc20a1 protein (DKPLRRNNSYTSY[T/I]MAICGMPLDSFRA), and the neoepitope presented on MHC-I molecules[36,37]. The IFN-γ$^+$ ELISPOT responses (Supplementary Fig. 24) in the splenocytes from mice treated with F_{13}-PEI/Mem (or together with anti-CTLA4) were significantly increased after this neoantigen resimulation, which demonstrates a successful establishment of the neoantigen-specific immune responses after vaccination with our F-PEI-based nanovaccines combined with tumour cell membranes.

Furthermore, the number of tumour-infiltrating CD8$^+$ T cells, which play a critical role in the antitumour immunity, was dramatically increased as the CD4$^+$Foxp3$^+$ T regulatory cells decreased in tumours on mice after the combined F_{13}-PEI/Mem + anti-CTLA4 treatment (Supplementary Fig. 25a–c). Meanwhile, more effector memory T cells (T_{EM}) were detected in the peripheral blood mononuclear cells of immunized mice (Supplementary Fig. 25d). To confirm the significance of T cells in the abscopal therapeutic response, T-cell blocking experiments were conducted using anti-CD8 antibody. After treatment with the CD8a monoclonal antibody (anti-CD8a), all the CD8$^+$ T cells in the blood were blockaded by anti-CD8a, whereas the CD8$^+$ T cells remained unaffected in mice treated with mouse monoclonal IgG (Fig. 5h). As expected, the blocking of CD8$^+$ T cells dramatically impaired the therapeutic efficacy of F_{13}-PEI/Mem vaccination + anti-CTLA4 treatment in inhibiting opposite tumours, which indicates that the adoptive immune responses through tumour-infiltrating CD8$^+$ T cells are important to the abscopal effect in our treatment strategy (Fig. 5i).

Fluoropolymer-based personalized nanovaccine for treating post-surgical orthotopic breast tumour metastases

Here, we propose a personalized cancer vaccine combined with ICB therapy for post-surgical immunotherapy of the recurrent tumours. Therefore, an orthotopic breast tumour model with spontaneous metastases was created by inoculating 4T1 tumour cells that expressed firefly luciferase (4T1-Luc) into the breast pad of each BALB/c mouse (Fig. 6a). To track the metastases of 4T1-Luc tumour cells, in vivo bioluminescence imaging was carried out every 5 days after day 10 (Fig. 6b). Compared with mice vaccinated with Mem only, vaccination with F_{13}-PEI/Mem could partly delay the tumour metastases. Of the 8 mice, 2 became tumour free and survived up

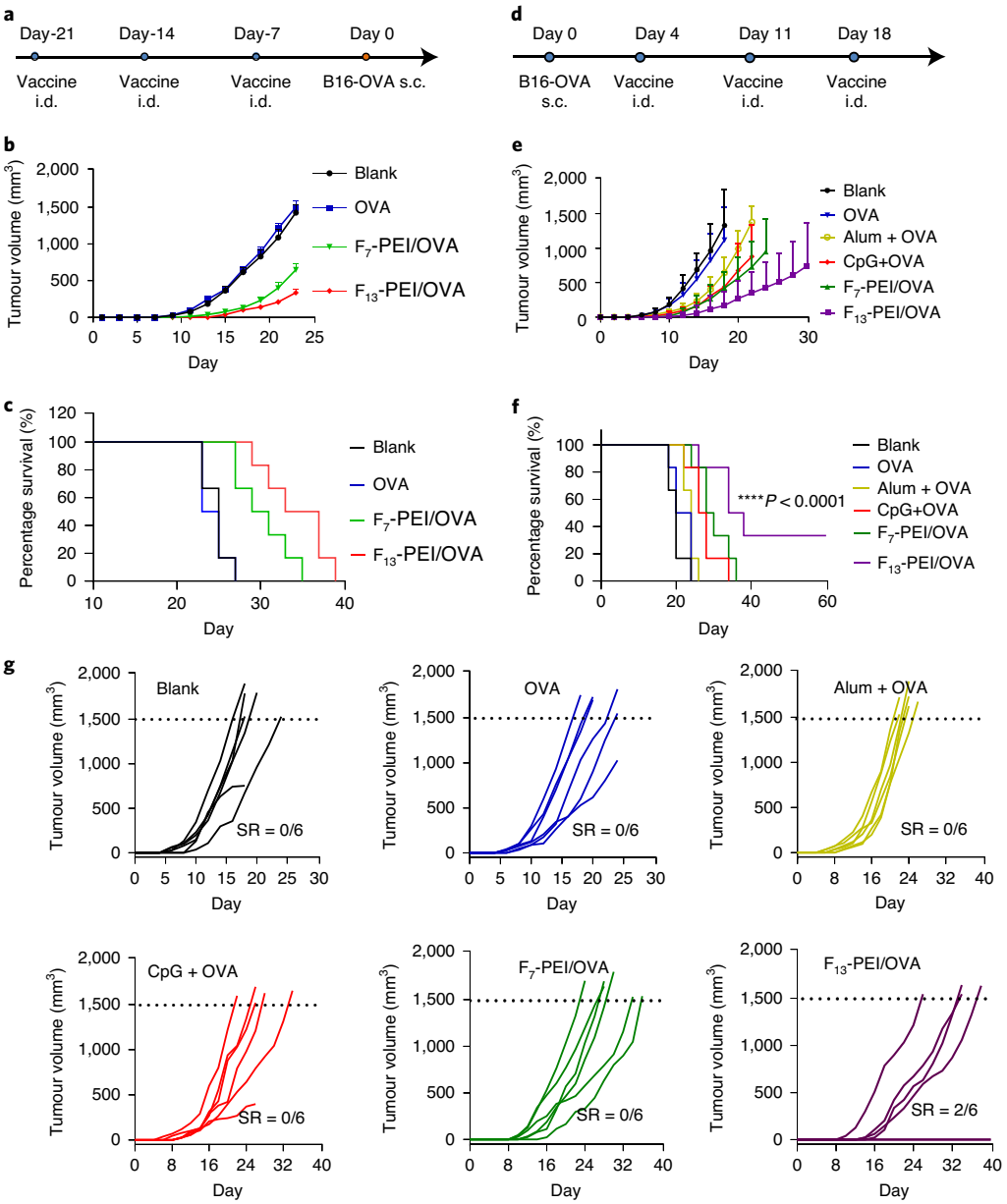

Fig. 4 | F_{13}-PEI/OVA nanovaccine inhibits tumour growth and prolongs survival in tumour-bearing mice. a–c, The prophylactic effects of F-PEI/OVA-based nanovaccines against B16-OVA melanoma. **d–f**, Antitumour therapeutic effect of F-PEI/OVA nanovaccines. **a**,**d**, Schemes of tumour challenge experiment design. **b**,**e**, Average tumour growth curves for B16-OVA tumours on mice after the various treatments indicated ($n = 6$ biologically independent mice for each group). Growth curves represent means ± s.e.m. **c**,**f**, Morbidity-free survival of different groups of mice with B16-OVA tumours after various treatments. Survival curves were obtained using the Kaplan–Meier method and compared by the log-rank test. ****$P < 0.0001$. **g**, Individual tumour growth curves in **e**. s.c., subcutaneous. SR, survival rate.

to 120 days (Fig. 6c). Moreover, although anti-CTLA4 treatment alone appeared to be not so effective, F_{13}-PEI/Mem vaccination combined with anti-CTLA4 showed impressive therapeutic effects in inhibiting tumour metastases. The survival rate in this group also showed a dramatic increase to 62.5% (5 of the 8 mice) within 120 days (Fig. 6c), which demonstrates the great promise of combining fluoropolymer-based personalized cancer vaccines with ICB therapy to treat post-surgical tumour metastases, a major challenge in clinical cancer treatment.

To assess the immune memory effects, mice that survived on day 120 after the first 4T1-Luc tumour-cell challenge in the F_{13}-PEI/Mem + anti-CTLA4 group were rechallenged with 4T1-Luc cells. Compared with the untreated mice, the tumour growth on the mice that survived after combination therapy (F_{13}-PEI/Mem + anti-CTLA4) appeared to be much slower (Fig. 6d). In fact, 2 of the 5 mice in this group showed no reoccurrence of the secondary tumour and all the mice exhibited extended survival compared to that of the age-matched control mice (Fig. 6e).

To further verify the immunological memory responses induced by our vaccination-based combination therapy, on day 120, peripheral blood mononuclear cells were collected to assess the memory $CD8^+$ T cells. Intriguingly, for the mice that survived to 120 days after the first 4T1-Luc tumour cell challenge (F_{13}-PEI/Mem + anti-CTLA4), the percentage of T_{EM} and central memory T cells (T_{CM}) in the $CD3^+CD8^+$ T cells showed a significant increase compared with that in the control mice (Fig. 6f–h

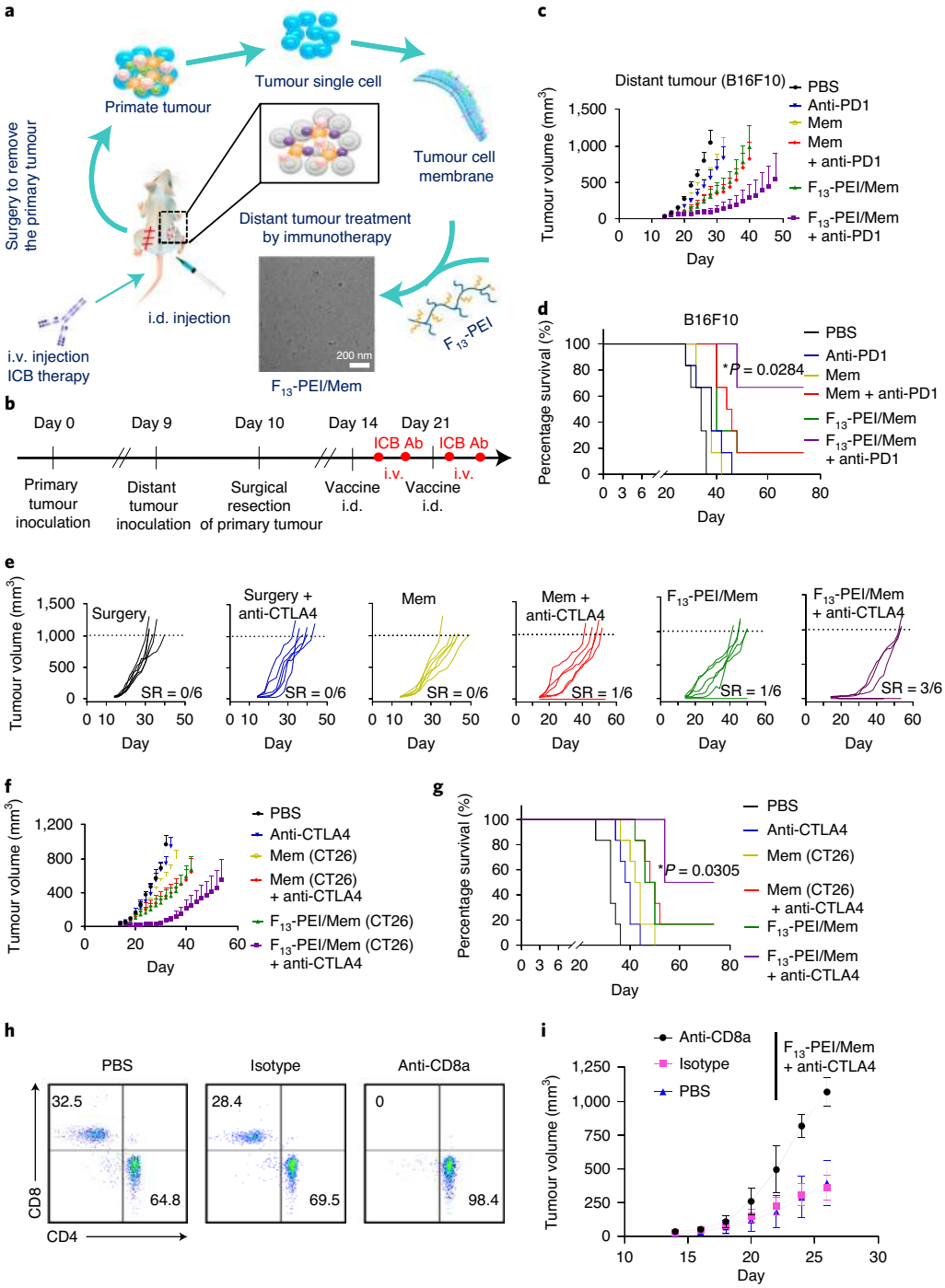

Fig. 5 | F_{13}-PEI/Mem nanovaccine synergy with ICB therapies to treat distant tumours post-surgery. a,**b**, Scheme (**a**) and timeline (**b**) to show the preparation of F_{13}-PEI/Mem NPs from tumour cell membranes obtained from surgically resected tumours as personalized tumour nanovaccines, which were used in combination with ICB therapy to inhibit the growth of the tumour on the opposite side of each mouse. **c**,**d**, Distant tumour growth curves (**c**) of B16F10 tumours and morbidity-free survival of different groups of mice (**d**) with various treatments. **e**–**g**, Individual distant tumour growth curves (**e**), distant tumour average growth curves (**f**) of CT26 tumours, and morbidity-free survival (**g**) of different groups of mice after various treatments. **h**, Flow cytometry analysis of blood T cells 3 days after treatment with anti-CD8a or an isotype monoclonal antibody as control. Data shown are representative of six biologically independent mice. **i**, Distant tumour growth curves of tumour-bearing mice pre-treated with either anti-CD8a or an isotype monoclonal antibody followed by the combined F_{13}-PEI/Mem + anti-CTLA4 therapy. **b**,**f**,**i**, Data presented as mean ± s.e.m. **c**–**g**,**i**, $n = 6$ biologically independent mice for each group. **d**,**g**, Survival curves were obtained using the Kaplan–Meier method and compared by the log-rank test. *$P < 0.05$. Ab, anti-PD1 or anti-CTLA-4; i.v., intravenous.

and Supplementary Fig. 26). Furthermore, one week after the mice were rechallenged with 4T1-Luc tumour cells, the serum levels of both TNF-α and IFN-γ (Fig. 6i,j) were significantly increased in this group (F_{13}-PEI/Mem + anti-CTLA4).

Conclusions

In this work, we report a new strategy to fabricate tumour nanovaccines based on fluoroalkane-grafted cationic polymers, F-PEI. Such F-PEIs self-assemble with protein antigens or tumour cell

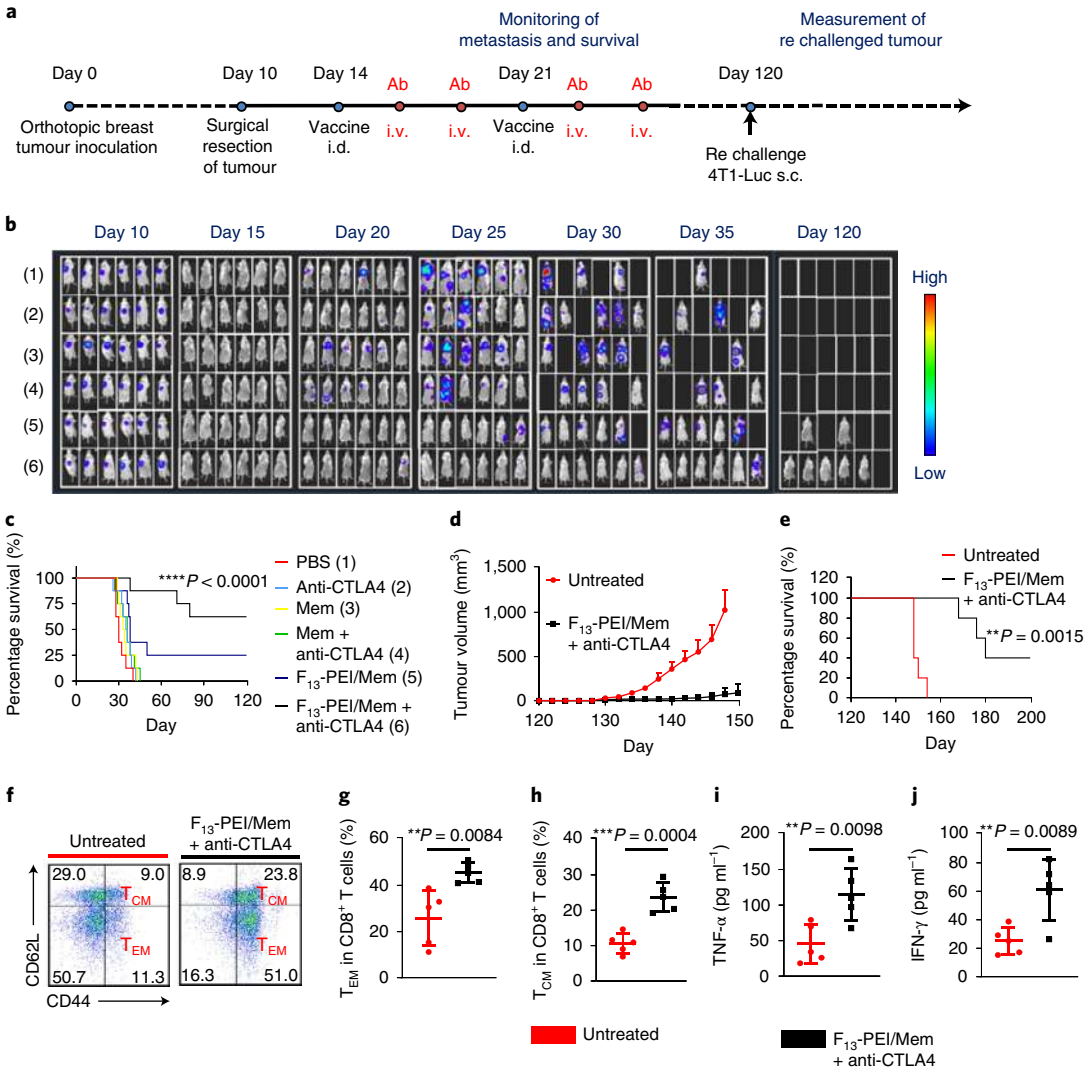

Fig. 6 | F_{13}-PEI/Mem nanovaccine synergy with ICB therapy and the long-term memory immune response to treat orthotopic 4T1 tumours post-surgery. **a**, Schematic illustration of the post-surgery personalized vaccine with anti-CTLA4 therapy to inhibit spontaneous tumour metastases in the orthotopic 4T1 breast tumour model. In different groups of mice, surgery was conducted to remove their primary orthotopic breast tumours followed by different post-surgical treatments, as indicated in **b**. **b**, In vivo bioluminescence images to track the metastases of 4T1-Luc breast cancer cells after surgery (only 6 of the 8 mice in each group are presented due to the limited figure space). **c**, Survival of mice that had orthotopic 4T1 tumours with spontaneous metastases after various post-surgical treatments ($n = 8$ biologically independent mice for each group). **d**–**j**, Mice that survived after the post-surgical combined F_{13}-PEI/Mem + anti-CTLA4 treatment were rechallenged with 4T1-Luc cells on day 120. Age-matched untreated mice were used as the control. **d**,**e**, Tumour growth curves (**d**) and morbidity-free survival (**e**) of mice ($n = 5$ biologically independent mice for each group). **d**, Data presented as mean ± s.e.m. **c**,**e**, Survival curves were obtained using the Kaplan–Meier method and compared by the log-rank test. $^{*}P < 0.05$, $^{**}P < 0.01$, $^{***}P < 0.001$, $^{****}P < 0.0001$. **f**–**h**, Representative flow dot plots (**f**) and statistical data of T_{EM} (**g**) and T_{CM} (**h**) in the peripheral blood analysed by flow cytometry (gated on $CD3^+CD8^+$ T cells) on day 120, immediately before rechallenging the mice with secondary tumours. **i**,**j**, TNF-α (**i**) and IFN-γ (**j**) levels in sera from mice isolated 7 days after the mice were rechallenged with secondary tumours. **g**–**j**, $n = 5$ biologically independent mice for each group. Data presented as mean ± s.d. Statistical significance between the indicated groups was determined using two-sided unpaired t-tests. $^{**}P < 0.01$, $^{***}P < 0.001$, $^{****}P < 0.0001$.

membrane antigens on simple mixing to form NPs with uniform sizes. Importantly, such fluoropolymer-based nanovaccines showed superior efficiencies in triggering antitumour immune responses compared those of vaccines using conventional immune adjuvants, such as CpG and alum, probably owing to their cytosolic antigen delivery ability to facilitate antigen cross-presentation, in addition to their ability to trigger DC activation, such as by stimulating the TLR4 signalling pathway. Therefore, F-PEI, by utilizing the unique hydrophobic and lipophobic chemical properties of fluoroalkane chains, is a unique type of antigen carrier and immune adjuvant to construct nanovaccines.

We found in our study that the tumour-specific immune responses triggered by fluoropolymer-based nanovaccines could be further amplified by ICB therapy. In particular, by utilizing the ability of fluoropolymer to package tumour cell membranes, personalized antitumour vaccines could be prepared by mixing F_{13}-PEI with cancer cell membranes separated from the resected tumour. As demonstrated in two subcutaneous tumour models and an orthotopic tumour model with spontaneous metastasis, such F_{13}-PEI/Mem personalized nanovaccines in combination with ICB therapy were able to treat metastatic tumours that cannot be completely removed by surgery. Furthermore, we observed a strong

immune-memory effect to effectively protect the cured mice from tumour rechallenge. Such an enhanced personalized anticancer vaccine synergy with ICB therapy may have great value in personalized post-surgical cancer immunotherapy for clinical translation.

In addition to the fabrication of personalized cancer vaccines using surgically resected tumours, the local administration of F_{13}-PEI into tumours post-tumour ablation therapies, such as high-intensity focused ultrasound (HIFU) therapy (Supplementary Fig. 27), may enable in situ generation of cancer vaccines from tumour debris to achieve a strong abscopal effect to inhibit the growth of distant tumours. Beyond protein-based and cell-membrane-based vaccines demonstrated in this work, these fluoropolymers may be used in the development of nucleic acid-based vaccines (for example, mRNA vaccines), for which cross-membrane delivery, DC activation and antigen presentation are essential processes. Moreover, beyond vaccines against cancer, such fluoropolymer may be further extended to the fabrication of other types of important vaccines, for example, vaccines against viral infections such as COVID-19.

Online content

Any methods, additional references, Nature Research reporting summaries, source data, extended data, supplementary information, acknowledgements, peer review information; details of author contributions and competing interests; and statements of data and code availability are available at https://doi.org/10.1038/s41565-020-00781-4.

Received: 27 July 2019; Accepted: 16 September 2020;
Published online: 2 November 2020

References

1. Klevorn, L. E. & Teague, R. M. Adapting cancer immunotherapy models for the real world. *Trends Immunol.* **37**, 354–363 (2016).
2. Littman, D. R. Releasing the brakes on cancer immunotherapy. *Cell* **162**, 1186–1190 (2015).
3. Wang, C., Ye, Y., Hu, Q., Bellotti, A. & Gu, Z. Tailoring biomaterials for cancer immunotherapy: emerging trends and future outlook. *Adv. Mater.* **29**, 1606036 (2017).
4. Lu, J. et al. Nano-enabled pancreas cancer immunotherapy using immunogenic cell death and reversing immunosuppression. *Nat. Commun.* **8**, 1811 (2017).
5. Brahmer, J. R. et al. Phase I study of single-agent anti-programmed death-1 (MDX-1106) in refractory solid tumors: safety, clinical activity, pharmacodynamics, and immunologic correlates. *J. Clin. Oncol.* **28**, 3167–3175 (2010).
6. Chao, Y. et al. Combined local immunostimulatory radioisotope therapy and systemic immune checkpoint blockade imparts potent antitumour responses. *Nat. Biomed. Eng.* **2**, 611–621 (2018).
7. Weichselbaum, R. R., Liang, H., Deng, L. & Fu, Y. X. Radiotherapy and immunotherapy: a beneficial liaison? *Nat. Rev. Clin. Oncol.* **14**, 365–379 (2017).
8. Chen, Q. et al. In situ sprayed bioresponsive immunotherapeutic gel for post-surgical cancer treatment. *Nat. Nanotechnol.* **14**, 89–97 (2019).
9. Wang, C. et al. In situ activation of platelets with checkpoint inhibitors for post-surgical cancer immunotherapy. *Nat. Biomed. Eng.* **1**, 0011 (2017).
10. Rosenberg, S. A., Yang, J. C. & Restifo, N. P. Cancer immunotherapy: moving beyond current vaccines. *Nat. Med.* **10**, 909–915 (2004).
11. Yarchoan, M., Johnson, B. A. III, Lutz, E. R., Laheru, D. A. & Jaffee, E. M. Targeting neoantigens to augment antitumour immunity. *Nat. Rev. Cancer* **17**, 209–222 (2017).
12. Guo, Y., Lei, K. & Tang, L. Neoantigen vaccine delivery for personalized anticancer immunotherapy. *Front. Immunol.* **9**, 1499 (2018).
13. Zhu, G., Zhang, F., Ni, Q., Niu, G. & Chen, X. Efficient nanovaccine delivery in cancer immunotherapy. *ACS Nano* **11**, 2387–2392 (2017).
14. Luo, M. et al. A STING-activating nanovaccine for cancer immunotherapy. *Nat. Nanotechnol.* **12**, 648–654 (2017).
15. Kuai, R., Ochyl, L. J., Bahjat, K. S., Schwendeman, A. & Moon, J. J. Designer vaccine nanodiscs for personalized cancer immunotherapy. *Nat. Mater.* **16**, 489–496 (2016).
16. Rodriguez, A., Regnault, A., Kleijmeer, M., Ricciardi-Castagnoli, P. & Amigorena, S. Selective transport of internalized antigens to the cytosol for MHC class I presentation in dendritic cells. *Nat. Cell Biol.* **1**, 362–368 (1999).
17. Cruz, F. M., Colbert, J. D., Merino, E., Kriegsman, B. A. & Rock, K. L. The biology and underlying mechanisms of cross-presentation of exogenous antigens on MHC-I molecules. *Annu. Rev. Immunol.* **35**, 149–176 (2017).
18. Lv, S. et al. Nanoparticles encapsulating hepatitis B virus cytosine-phosphate-guanosine induce therapeutic immunity against HBV infection. *Hepatology* **59**, 385–394 (2014).
19. Yang, J., Zhang, Q., Chang, H. & Cheng, Y. Surface-engineered dendrimers in gene delivery. *Chem. Rev.* **115**, 5274–5300 (2015).
20. Zhang, Z. et al. The fluorination effect of fluoroamphiphiles in cytosolic protein delivery. *Nat. Commun.* **9**, 1377 (2018).
21. Cametti, M., Crousse, B., Metrangolo, P., Milani, R. & Resnati, G. The fluorous effect in biomolecular applications. *Chem. Soc. Rev.* **41**, 31–42 (2012).
22. Stewart, M. P., Langer, R. & Jensen, K. F. Intracellular delivery by membrane disruption: mechanisms, strategies, and concepts. *Chem. Rev.* **118**, 7409–7531 (2018).
23. Janeway, C. A. Jr & Bottomly, K. Signals and signs for lymphocyte responses. *Cell* **76**, 275–285 (1994).
24. Folks, T. M. et al. Tumor necrosis factor alpha induces expression of human immunodeficiency virus in a chronically infected T-cell clone. *Proc. Natl Acad. Sci. USA* **86**, 2365–2368 (1989).
25. Dienz, O. & Rincon, M. The effects of IL-6 on CD4 T cell responses. *Clin. Immunol.* **130**, 27–33 (2009).
26. Lanzavecchia, A. & Sallusto, F. Regulation of T cell immunity by dendritic cells. *Cell* **106**, 263–266 (2001).
27. He, W. et al. Re-polarizing myeloid-derived suppressor cells (MDSCs) with cationic polymers for cancer immunotherapy. *Sci. Rep.* **6**, 24506 (2016).
28. Hornung, V. et al. Silica crystals and aluminum salts activate the NALP3 inflammasome through phagosomal destabilization. *Nat. Immunol.* **9**, 847–856 (2008).
29. Yamamoto, A. et al. Bafilomycin A prevents maturation of autophagic vacuoles by inhibiting fusion between autophagosomes and lysosomes in rat hepatoma cell line, H-4-II-E cells. *Cell Struct. Funct.* **23**, 33–42 (1998).
30. Wang, M., Liu, H., Li, L. & Cheng, Y. A fluorinated dendrimer achieves excellent gene transfection efficacy at extremely low nitrogen to phosphorus ratios. *Nat. Commun.* **5**, 3053 (2014).
31. Bevan, M. J. Helping the $CD8^+$ T-cell response. *Nat. Rev. Immunol.* **4**, 595–602 (2004).
32. Yang, R. et al. Cancer cell membrane-coated adjuvant nanoparticles with mannose modification for effective anticancer vaccination. *ACS Nano* **12**, 5121–5129 (2018).
33. Kroll, A. V. et al. Nanoparticulate delivery of cancer cell membrane elicits multiantigenic antitumor immunity. *Adv. Mater.* **29**, 1703969 (2017).
34. Ochyl, L. J. et al. PEGylated tumor cell membrane vesicles as a new vaccine platform for cancer immunotherapy. *Biomaterials* **182**, 157–166 (2018).
35. Grosso, J. F. & Jure-Kunkel, M. N. CTLA-4 blockade in tumor models: an overview of preclinical and translational research. *Cancer Immunol. Res.* **13**, 5 (2013).
36. D'Alise, A. M. et al. Adenoviral vaccine targeting multiple neoantigens as strategy to eradicate large tumors combined with checkpoint blockade. *Nat. Commun.* **10**, 2688 (2019).
37. Li, A. W. et al. A facile approach to enhance antigen response for personalized cancer vaccination. *Nat. Mater.* **17**, 528–534 (2018).

Methods

Materials. Branched PEI with a molecular weight of 25 kDa was obtained from Sigma-Aldrich. 3-(perfluoropropyl)-1,2-propenoxide and 3-(perfluorohex-1-yl)-1,2-propenoxide were obtained from J&K Scientific. 3-(4,5-Dimethylthiazol-2-yl)-2,5-diphenyltetrazoliumbromide (MTT) was purchased from Sangon Biotech. OVA, $OVA_{257–263}$ (SIIEFNKL) peptide and CpG oligodeoxynucleotides were obtained from InvivoGen. Injective alum and bicinchonic acid kits were obtained from Thermo Scientific. LPS was purchased from Sigma-Aldrich. The inhibitors, which included dynasore and genistein, were purchased from MedChemExpress. Phycoerythrin (PE) -labelled SIINFEKL-MHC I tetramer was purchased from MBL. Antibodies used in this study are listed in Supplementary Table 2. The Slc20a1 peptide (DKPLRRNNSYTSYIMAICGMPLDSFRA) was synthesized by GenScript.

Synthesis of F_7-PEI and F_{13}-PEI. Functionalized PEIs were synthesized by the dropwise addition of epoxides that bore fluoroalkanes into PEI in methanol at a feeding ratio of 36: 1. The solutions were stirred at room temperature for 48 h. The products were purified by intensive dialysis against methanol and double-distilled water (molecular weight cutoff 3,500 Da), and then lyophilized for characterization.

Preparation and characterization of F_7-PEI/OVA and F_{13}-PEI/OVA NPs. The synthesized F_7PEI and F_{13}-PEI amphiphiles were mixed with OVA in deionized water at different weight ratios for 30 min. The sizes and zeta potentials of the formed F_7-PEI/OVA and F_{13}-PEI/OVA NPs were measured with a Zetasizer Nano ZS (Malvern Instruments). The morphology of the NPs was observed with an FEI Tecnai F20 transmission electron microscope.

Animals and cells. Female C57BL/6 mice (6–8 weeks) and female BALB/c mice (6–8 weeks) were purchased from Nanjing Pengsheng Biological Technology Co., Ltd. Female OT-I transgenic mice (6–8 weeks) were a gift from X. Wang, Soochow University. Female gene knockout *Tlr4*$^{-/-}$ mice were purchased from GemPharmatech Co., Ltd. Mice were housed in groups of 5 mice per individually ventilated cage in a 12 h light–dark cycle (8:00–20:00 light; 20:00–8:00 dark), with constant room temperature (21 ± 1 °C) and relative humidity (40–70%). All the mice had access to food and water ad libitum. The animal procedures were performed with ethical compliance and approval by the Institutional Animal Care and Use Committee at Soochow University. DC2.4 cells (a gift from C. Wang, Soochow University), B16-OVA cells (a gift from H. Liu, Soochow University) and B16F10 cells (Cell Bank, Shanghai Institutes for Biological Sciences, Chinese Academy of Sciences) were cultured in DMEM (HyClone) with high glucose that contained 10% fetal bovine serum (FBS; Gibco) and 1% penicillin sulfate and streptomycin (PS, HyClone) at 37 °C in 5% CO_2. CT26 cells (Cell Bank, Shanghai Institutes for Biological Sciences, Chinese Academy of Sciences) and 4T1-Luc cells (a gift from PerkinElmer Co.) were cultured in Roswell Park Memorial Institute (RPMI) 1640 media (HyClone) that contained 10% FBS (Gibco) and 1% PS at 37 °C in 5% CO_2. HEK-Dual Null (NF/IL8) cells (InvivoGen) were cultured with DMEM that contained 4.5 g l^{-1} glucose, 2 mM L-glutamin, 10% FBS and 1% PS supplemented with 100 μg ml^{-1} Normocin (Invitrogen) and 50 mg ml^{-1} Zeocin (Invitrogen) at 37 °C in 5% CO_2. HEK-Dual mTLR4 (NF/IL8) cells (InvivoGen) were cultured with DMEM that contained 4.5 g l^{-1} glucose, 2 mM L-glutamin, 10% FBS and 1% PS supplemented with 100 μg ml^{-1} Hygromycin B Gold (InvivoGen), 100 μg ml^{-1} Normocin and 50 μg ml^{-1} Zeocin at 37 °C in 5% CO_2. The identity of the cell lines was frequently checked by their morphological features. All the cell lines were tested to be mycoplasma-free by their suppliers. No mycoplasma contamination was found before use.

In vitro cytotoxicity assessment, cross-presentation and DC maturation assay. BMDCs were differentiated from bone marrow cells isolated from the femurs and tibias of 6-week-old C57BL/6 mice according to an established method[38]. Non-adherent and loosely adherent cells with a maturation level of about 20% (percentage of $CD86^+CD80^+$ cells in $CD11c^+$ cells) on day 7 were collected and used for the studies. The cytotoxicities of PEI/OVA, F_7-PEI/OVA and F_{13}-PEI/OVA NPs were first measured by a well-established MTT assay. Generally, BMDCs incubated with F_7-PEI/OVA and F_{13}-PEI/OVA NPs at various concentrations were seeded in a 96-well plate at a density of around 5×10^4 cells for 24 h. Only the OVA, F_7-PEI/OVA and F_{13}-PEI/OVA NPs at various concentration formulations without BMDCs are shown as the controls. Then, a standard MTT assay was used to determine the relative cell viability.

To assess DC cross-presentation, 10^6 ml^{-1} BMDCs were pulsed with OVA (10 μg ml^{-1}), F_7-PEI/OVA NPs ([OVA] = 10 μg ml^{-1}) or F_{13}-PEI/OVA NPs ([OVA] = 10 μg ml^{-1}) with different F-PEI:OVA ratios for 12 h. After various treatments, BMDCs were harvested, resuspended in flow cytometry (fluorescence-activated cell sorting (FACS)) buffer (PBS that contained 1% FBS), incubated with anti-CD16/32 at room temperature and stained with anti-SIINFEKL-H-2Kb-APC and anti-CD11c-FITC before analysis by flow cytometry (BD Accurit TM C6 Plus).

For in vitro DC maturation experiments, 10^6 ml^{-1} immature DCs were plated into 24-well non-treated dishes (Nunc) and simulated with OVA (10 μg ml^{-1}), F_7-PEI/OVA NPs ([OVA] = 10 μg ml^{-1}) or F_{13}-PEI/OVA NPs ([OVA] = 10 μg ml^{-1}) with different F-PEI:OVA ratios for 12 h. After various treatments, BMDCs were harvested, resuspended in flow cytometry (FACS) buffer (PBS that contained 1% FBS), incubated with anti-CD16/32 at room temperature and then stained with fluorophore-labelled antibodies against CD11c, CD86, CD80, CD40 and MHC-II for 30 min before analysis by flow cytometry (BD Accurit C6 Plus) and by FlowJo software. The supernatant was collected to measure cytokine TNF-α, IL-6 and IL-12p70 levels an using enzyme-linked immunosorbent assay (ELISA) assay according to the manufacturer's protocols (Invitrogen).

In vitro $CD8^+$ T-cell priming assay. Briefly, BMDCs were incubated with OVA ([OVA] = 10 μg ml^{-1}), F_7-PEI/OVA ([F_7-PEI] = 10 μg ml^{-1}, [OVA] = 10 μg ml^{-1}) or F_{13}-PEI/OVA ([F_7-PEI] = 10 μg ml^{-1}, [OVA] = 10 μg ml^{-1}) NPs at 37 °C for 12 h. The treated BMDCs were then washed by PBS that contained 0.1% BSA. $CD8^+$ T lymphocytes from OT-I mice negatively selected by magnetic separation (MACS system, Miltenyi Biotec), according to the manufacturer's instructions, were stained with the CellTrace CFSE Cell Proliferation Kit (Invitrogen) according to the vendors' protocol. Treated DCs (10^5 ml^{-1}) were then mixed with CFSE-stained splenic $CD8^+$ T cells at a DC:T-cell ratio of 1:10 and incubated in round-bottom 96-well plates (Beyotime) for 72 h. Cells were washed by PBS that contained 1% FBS, incubated with anti-CD16/32 at room temperature and stained with anti-CD3-PE and anti-CD8a-APC, and finally analysed by FACS. The supernatant was collected and analysed for cytokine TNF-α and IFN-γ by ELISA according to the manufacturer's protocols (Invitrogen).

In vitro cellular uptake and intracellular localization of antigens. To assess the cellular uptake of OVA, F_7-PEI/OVA and F_{13}-PEI/OVA by BMDCs, 10^6 ml^{-1} immature wt BMDCs or *Tlr4*$^{-/-}$ BMDCs were plated in 24-well dishes and stimulated with FITC-labelled OVA (10 μg ml^{-1}), F_7-PEI/OVA-FITC NPs ([F_7-PEI] = 10 μg ml^{-1}, [OVA-FITC] = 10 μg ml^{-1}) or F_{13}-PEI/OVA-FITC NPs ([F_{13}-PEI] = 10 μg ml^{-1}, [OVA-FITC] = 10 μg ml^{-1}) for 12 h. BMDCs were harvested and trypan blue was added to quench the extracellular fluorescence. After washing three times, the treated BMDCs were incubated with anti-CD16/32 for 30 min at 4 °C before being stained with anti-CD11c-FITC-APC, to analyse the cellular uptake using a flow cytometer (BD Accurit C6 Plus). To elucidate the endocytosis pathways, wild BMDCs were incubated with endocytosis inhibitors dynasore (80 μM) or genistein (700 μM) for 30 min before the addition of F_7-PEI/OVA-FITC or F_{13}-PEI/OVA-FITCNPs. The untreated cells were tested as the control.

For the endosomal escape test, DC2.4 cells were treated with the F_7-PEI/OVA-FITC or F_{13}-PEI/OVA-FITC complexes for 2, 4 or 6 h, and then washed with PBS three times. The lysosome and nuclei were stained with Lyso-tracker red (200 nM) and Hoechst 33342, respectively. After being washed with PBS, the cells were observed with a laser scanning confocal microscope (LSM 880, Carl Zeiss). The weight ratio of F_7-PEI or F_{13}-PEI to OVA-FITC was 1:1.

The fluorinated polymer (F_7-PEI or F_{13}-PEI) was mixed with rhodamine B isothiocyanate (RB) at a molar ratio of 1:3 for fluorescent labelling. DC2.4 cells were incubated with F_7-PEI-RB /OVA-FITC or F_{13}-PEI-RB/OVA-FITC complexes for 30 min and the excess F-PEI-RB/OVA-FITC complexes were washed away with PBS. After that, the treated cells were incubated at 37 °C and observed with a laser scanning confocal microscope (LSM 880, Carl Zeiss) at indicated time intervals. The weight ratio of F_7-PEI-RB or F_{13}-PEI-RB to OVA-FITC was 1:1. Bafilomycin A1 (50 nM) (Yuanye Bio-Technology) was used to treat the DC2.4 cells for 1 h before adding the F-PEI/OVA-FITC complex to further investigate the endosomal escape behaviours of the vectors.

Endotoxin-level measurement. Endotoxin levels of various F-PEI-based formulations without dilution were detected according to the manufacturer's protocols using the chromogenic LAL endotoxin assay kit (GenScript). According to US Food and Drug Administration guidelines, sterile water for injection and irrigation has an allowable endotoxin limit of 0.25 EU ml^{-1}.

LN analysis. The inguinal LNs were dissected from the vaccinated mice, and then processed through mechanical disruption before digestion for 30 min at 37 °C in RPMI-1640 (10% heat-inactivated FBS and 1% PS) that contained 1.5 mg ml^{-1} collagenase IV(Sigma), 1.5 mg ml^{-1} collagenase I (Sigma), 1.5 mg ml^{-1} hyaluronidase (Sigma) and 0.2 mg ml^{-1} DNase I (Sigma). The samples were then passed through 200-mesh nylon mesh filters to obtain single-cell suspensions, which were incubated with anti-CD16/32 for 30 min at 4 °C before being stained with anti-CD11c-APC, anti-CD86-PE and anti-CD80-PE/Cy7 to analyse DC maturation. For the analysis of DC cross-presentation, the obtained single-cell suspensions were incubated with anti-CD16/32 at room temperature before staining with anti-CD11c-FITC and anti-SIINFEKL/H-2Kb-APC. Flow data were acquired on a flow cytometer (BD Accurit C6 Plus) and analysed by FlowJo software.

ELISA assay. IL-1β from the supernatant of BMDCs after treatment with F-PEI/OVA and IFN-γ from serum of the vaccinated mice were determined by ELISA kits (Invitrogen) following standard protocols. The levels of OVA-specific IgG_1 and IgG_{2a} in the serum were also measured by ELISA following a literature protocol[38].

Tetramer analysis and peptide re-stimulation of splenocytes. The splenocytes were isolated by mincing the spleen from the immunized mice through 200-mesh

cell strainers and the red blood cells (RBCs) were then lysed using RBC lysis buffer. Splenocytes stained with phycoerythrin-labelled SIINFEKL-MHC I tetramer, anti-CD8-APC and anti-CD3-FITC were analysed for the percentages of OVA-specific $CD8^+$ T cells using the tetramer staining assay following the standard protocol.

For ELISPOT evaluations (BD Biosciences), 5×10^5 splenocytes were seeded into each well in duplicate and incubated with antigens (10 μg ml^{-1} $OVA_{257–264}$ peptides) or Slc20a1 peptide (DKPLRRNNSYTSYIMAICGMPLDSFRA). The plates were kept at 37 °C in 5% CO_2 for 24 h. Following the vendor's protocol, an automated ELISPOT Plate Reader (AID iSpot) was used to determine the amount of IFN-γ SFCs and the data presented as SFC per one million cells or SFC per 0.5 million cells.

To demonstrate the cellular responses, 10^6 splenocytes collected from immunized mice were incubated with $OVA_{257–264}$ peptide (10 μg ml^{-1}) in the presence of brefeldin A and monensin for 6 h. Then, the cells were stained with anti-CD3-FITC, anti-IFN-γ-APC and anti-CD8-PE according to the intracellular staining protocol before the flow cytometry measurement (BD Accurit C6 Plus).

Prophylactic and therapeutic studies with OVA-based nanovaccines. For the prophylactic study, different vaccines were intradermally injected at the tail base into the female C57BL/6 mice of each group at one week intervals three times. Seven days after the final vaccination, the vaccinated mice were subcutaneously challenged with 3×10^5 B16-OVA cells. The tumour volume was measured with a caliper every other day and calculated according to following the formula: V = length × width × width/2 (mm^3). Mice were euthanized when the tumour volume reached 1,500 mm^3.

For the therapeutic study, female C57BL/6 mice (6 weeks old) were subcutaneously injected with 3×10^5 B16-OVA cells. Female C57BL/6 mice were intradermally vaccinated with different kinds of vaccines, as described in the main text, on days 4, 11 and 18. Mice were euthanized when the tumour volumes reached 1,500 mm^3.

Biodistribution of F_{13}-PEI/OVA NPs. To investigate their biodistribution, F_{13}-PEI/OVA NPs were radiolabelled with ^{125}I (labelling on OVA) following the standard protocol and injected at the tail base of the mice. At different time points, major organs, such as the heart, liver, spleen, lung, kidney, inguinal LN and the injection site, were collected and weighed, and the radioactivity was measured with a gamma counter (LB211, Berthold Technologies GmbH & Co KG).

The in situ B16F10, CT26 and 4T1-Luc cell membrane derivation. Tumours with a weight of about 600 mg were resected from B16F10, CT26 and 4T1-Luc tumour-bearing mice. These tumour tissues were then processed through mechanical disruption and digested by 1.5 mg ml^{-1} collagenase IV (Sigma), 1.5 mg ml^{-1} collagenase I (Sigma), 1.5 mg ml^{-1} hyaluronidase (Sigma) and 0.2 mg ml^{-1} DNase I (Sigma) for 45 min at 37 °C. The cells were filtered through nylon 200-mesh filters and washed with FACS buffer. RBCs were lysed using RBC lysis buffer. The $CD45^+$ leukocyte cells were then removed from the obtained single-cell suspension using $CD45^+$ magnetic beads (Miltenyi Biotec)[39] and about 6×10^6 tumour cells could be collected. The obtained cell membranes were prepared by mechanical disruption in the presence of phosphatase inhibitor and protease inhibitor cocktails, as previously reported[33]. Then, the membranes were obtained by centrifugation at 14,800 r.p.m. for 25 min to remove the cell nuclei and cytoplasm. The resulting packed membrane was washed in 0.2 mM ethylenediaminetetraacetic acid in DNase free/RNase free water (Invitrogen). The total membrane protein content was quantified with a bicinchonic acid protein assay kit (Thermo Scientific).

Preparation and characterization of F_{13}-PEI/Mem NPs. The synthesized F_{13}-PEI amphiphiles were mixed with the obtained cancer cell membrane in deionized water at a weight ratio of 1:1 for 30 min. The sizes and zeta potentials of the formed F_{13}PEI-MemNPs were measured with a Zetasizer Nano ZS (Malvern Instruments). The morphology of the NPs was observed with a FEI Tecnai G20 TWIN cytotransmission electron microscope.

Membrane-based nanovaccine synergy with ICB therapeutic study post-surgery. To study the therapeutic effects of the F_{13}-PEI/Mem nanovaccine after surgery, B16F10 cells were transplanted into the left flanks of C57BL/6 mice. After 9 days, a second tumour as the distant tumour (5×10^5 B16F10) was inoculated into the right flank of each mouse. At day 10, mice were randomly divided into six groups for different treatments: blank (1), anti-PD1 (2), membrane (3), membrane + anti-PD1 (4), F_{13}-PEI/Mem (5) and F_{13}-PEI/Mem + anti-PD1 (6). Tumours in the left flanks of all the mice were resected by surgery to prepare the tumour cell membranes. On 4 (day 14) and 11 (day 21) days after surgery, the mice in groups 3 and 4 were intradermally vaccinated with membranes using a one-to-one correspondence. By simply mixing with the F_{13}-PEI, the obtained F_{13}-PEI/Mem formulations were intradermally injected into the surgical resection mice in groups 5 and 6 using one-to-one correspondence 4 (day 14) and 11 (day 21) days post-surgery. For groups 2, 4 and 6, the mice were intravenously administrated with anti-PD1 (20 μg per mouse for each injection) 5 (day 15), 8 (day 18), 12 (day 22) and 15 (day 25) days post-surgery. The sizes of the left tumour were measured every other day. Mice were euthanized when the tumour volumes reached 1,500 mm^3. Similar experiments were conducted for the CT26 tumour model, except that anti-CTLA4 (20 μg per mouse for each injection) was used to replace anti-PD1 for the treatment study. The sizes of the left tumour were measured every other day. Mice were euthanized when the tumour volumes reached 1,000 mm^3.

Tumour-infiltrating lymphocytes analysis. For analyses of the immune cells in distant tumours after the above immune combination therapy, tumours were resected from the CT26 tumour-bearing mice on day 21 (for the distant tumour, 10^6 CT26 tumour cells were injected on day 9). These tumour tissues were then processed through mechanical disruption, digested and filtered to obtain single-cell suspensions, which were then stained with antibodies according to our previous report for flow cytometry analysis[40]. For instance, a single-cell suspension was incubated with anti-CD16/32 and then stained with anti-CD45-Alexa Fluor 488, anti-CD3e-APC, anti-CD8a-Percp/Cy5.5 and anti-CD4-APC/Cy7 for 30 min at 4 °C before being fixed and permeabilized by eBioscience Foxp3/Transcription Factor Staining Buffer Set (eBioscience). Cells were then stained with anti-Foxp3-PE for 30 min at 4 °C and analysed using flow cytometry (BD FACS Verse).

T-cell blocking experiments. BALB/c mice that bore CT26 tumours were treated with F_{13}-PEI/Mem + anti-CTLA4 after surgery, as described before. The treated mice were intravenously injected with anti-mouse-CD8 (for $CD8^+$ T-cell depletion, 2.43, BioXcell) or mouse IgG (as Control, Southern Biotech) (20 μg per mouse), which were given three times, on days 0 (day 10), 5 (day 15) and 10 (day 20) after surgical removal of their first tumours. On day 3 (day 13) post-surgery, the blood T cells were collected to confirm the blockade of the CD8 T cells. The sizes of the tumours on the opposite side without surgery were measured every other day.

Orthotopic tumour model for F_{13}-PEI/Mem-triggered immunotherapy. To build the spontaneous metastatic 4T1 orthotopic murine breast cancer model, 2×10^6 4T1-Luc cells dispersed in PBS were injected into the breast pad of each BALB/c mouse. After ten days, we randomly divided the mice into six groups ($n=8$): (1) surgery, (2) surgery + anti-CTLA4, (3) membrane, (4) membrane + anti-CTLA4, (5) F_{13}-PEI/Mem and (6) F_{13}-PEI/Mem + anti-CTLA4. Tumours with the weight of 600 mg in the orthotopic breast pad of mice were resected. Membranes could be collected by hypotonic lysing, mechanical membrane disruption and differential centrifugation. On days 14 and 21, mice were vaccinated with membranes or F_{13}-PEI/Mem by intradermal injection. Mice in groups 2, 4 and 6 were intravenously administrated with anti-CTLA4 (10 μg per mouse for each injection) on days 15, 18, 22 and 25. Spontaneous metastases of tumour cells were monitored by an IVIS spectrum imaging system analysed by Living Image software (Perkin Elmer). On day 120, the mice that survived were subcutaneously injected 5×10^5 4T1-Luc cells to evaluate the immunological memory effect.

Immunological memory responses triggered by our combination therapy. For the analysis of memory T cells, circulating peripheral blood mononuclear cells from the peripheral blood were harvested from the survived mice and stained with anti-CD3-FITC, anti-CD8-PerCP-Cy5.5, anti-CD62L-APC and anti-CD44-PE. Data analysis was carried out using FlowJo software. One week after the 4T1-Luc cells inoculation (day 127), the cytokines, which included TNF-α (Invitrogen) and IFN-γ (Invitrogen) from sera, were determined by ELISA kits following the standard protocols.

Statistical analysis. All the values in the present study are presented as the mean ± s.d. unless otherwise indicated in the figure captions. One-way analysis of variance was used for multiple comparisons when more than two groups were compared, and Student's *t*-test was used for two-group comparisons. All the statistical analyses were carried out with GraphPad Prism software package (PRISM 8.0; GraphPad Prism Software), Excel 2016 or Excel 2019. Survival curves were obtained using the Kaplan–Meier method and compared by the log-rank test. The threshold for statistical significance was $P<0.05$.

Reporting summary. Further information on research design is available in the Nature Research Reporting Summary linked to this article.

Data availability

The main data supporting the results in this study are available within the paper and Supplementary Information. The raw and analysed datasets generated during the study are too large to be publicly shared, yet they are available for research purposes from the corresponding authors upon reasonable request.

References

38. Xu, L. et al. Morphologically virus-like fullerenol nanoparticles act as the dual-functional nanoadjuvant for HIV-1 vaccine. *Adv. Mater.* **25**, 5928–5936 (2013).
39. Issadore, D. et al. Self-assembled magnetic filter for highly efficient immunomagnetic separation. *Lab Chip* **11**, 147–151 (2011).

40. Xu, J. et al. Near-infrared-triggered photodynamic therapy with multitasking upconversion nanoparticles in combination with checkpoint blockade for immunotherapy of colorectal cancer. *ACS Nano* **11**, 4463–4474 (2017).

Acknowledgements

This work was partially supported by the National Key Research and Development (R&D) Program of China (2016YFA0201200, 2017YFE0131700 and 2019YFA0904500), the National Natural Science Foundation of China (51525203, 21725402 and 51761145041), the 111 Project, the Jiangsu Social Development Project (BE2019658), the Natural Science Foundation of Jiangsu Higher Education Institutions of China (19KJA310008) and the Collaborative Innovation Center of Suzhou Nano Science and Technology (Nano-CIC). The authors thank H. Liu for B16-OVA tumour cells and X. Wang for the OT-I mice. Our gratitude also goes to Y. Huang for valuable comments and suggestions.

Author contributions

Z.L., Y.C., R.P. and J.X. conceived the project and designed the experiments. Z.L. and R.P. supervised the project. Z.L., R.P. and J.X. wrote the manuscript. J.X., J.L., Q.Z., Z.Y., Z.C., P.P., C.W., H.W., Z.D. and Y.C. carried out the experiments. J.L. assisted in taking and analysing the microscope images. C.W. and K.Y. supported the operation and analysis of the flow cytometer. All the authors discussed the results and commented on the manuscript.

Competing interests

The authors declare no competing interests.

Additional information

Supplementary information is available for this paper at https://doi.org/10.1038/s41565-020-00781-4.

Correspondence and requests for materials should be addressed to R.P., Y.C. or Z.L.

Peer review information *Nature Nanotechnology* thanks Jeffrey Hubbell, Helder A. Santos and the other, anonymous, reviewer(s) for their contribution to the peer review of this work.

Reprints and permissions information is available at www.nature.com/reprints.

nature research

Corresponding author(s): Zhuang Liu

Last updated by author(s): Oct 9, 2020

Reporting Summary

Nature Research wishes to improve the reproducibility of the work that we publish. This form provides structure for consistency and transparency in reporting. For further information on Nature Research policies, see our Editorial Policies and the Editorial Policy Checklist.

Statistics

For all statistical analyses, confirm that the following items are present in the figure legend, table legend, main text, or Methods section.

n/a	Confirmed	
☐	☒	The exact sample size (*n*) for each experimental group/condition, given as a discrete number and unit of measurement
☐	☒	A statement on whether measurements were taken from distinct samples or whether the same sample was measured repeatedly
☐	☒	The statistical test(s) used AND whether they are one- or two-sided *Only common tests should be described solely by name; describe more complex techniques in the Methods section.*
☐	☒	A description of all covariates tested
☐	☒	A description of any assumptions or corrections, such as tests of normality and adjustment for multiple comparisons
☐	☒	A full description of the statistical parameters including central tendency (e.g. means) or other basic estimates (e.g. regression coefficient) AND variation (e.g. standard deviation) or associated estimates of uncertainty (e.g. confidence intervals)
☐	☒	For null hypothesis testing, the test statistic (e.g. *F*, *t*, *r*) with confidence intervals, effect sizes, degrees of freedom and *P* value noted *Give P values as exact values whenever suitable.*
☒	☐	For Bayesian analysis, information on the choice of priors and Markov chain Monte Carlo settings
☒	☐	For hierarchical and complex designs, identification of the appropriate level for tests and full reporting of outcomes
☐	☒	Estimates of effect sizes (e.g. Cohen's *d*, Pearson's *r*), indicating how they were calculated

Our web collection on statistics for biologists contains articles on many of the points above.

Software and code

Policy information about availability of computer code

Data collection	No software was used
Data analysis	All statistical analyses were performed on Graphpad Prism 8, Excel 2016 or Excel 2019. Living Image software (Perkin Elmer) was used to analyse bioluminescent images.All the flow cytometry data were processed using FlowJo (version 10.4., Becton, Dickinson & Company).

For manuscripts utilizing custom algorithms or software that are central to the research but not yet described in published literature, software must be made available to editors and reviewers. We strongly encourage code deposition in a community repository (e.g. GitHub). See the Nature Research guidelines for submitting code & software for further information.

Data

Policy information about availability of data

All manuscripts must include a data availability statement. This statement should provide the following information, where applicable:

- Accession codes, unique identifiers, or web links for publicly available datasets
- A list of figures that have associated raw data
- A description of any restrictions on data availability

The main data supporting the results in this study are available within the paper and its Supplementary Information. The raw and analysed datasets generated during the study are too large to be publicly shared, yet they are available for research purposes from the corresponding authors on reasonable request.

Field-specific reporting

Please select the one below that is the best fit for your research. If you are not sure, read the appropriate sections before making your selection.

☒ Life sciences ☐ Behavioural & social sciences ☐ Ecological, evolutionary & environmental sciences

For a reference copy of the document with all sections, see nature.com/documents/nr-reporting-summary-flat.pdf

Life sciences study design

All studies must disclose on these points even when the disclosure is negative.

Sample size	No statistical methods were used to predetermine the sample sizes. It is impossible to predict the magnitude of experimental variation between animals based on our current knowledge. The group sizes (at least three animals per treatment group) represents the minimum number animals needed to reach statistical significance ($p < 0.05$) between experimental groups.
Data exclusions	No data were excluded.
Replication	Experiment were repeated and experimental findings were reproducible. Details of experimental replicates are given in the figure legends. All reported attempts at replication were successful.
Randomization	All experimental samples or models were allocated randomly to each group.
Blinding	No blinding was done in this study. Most of the studies contained multiple steps (including the material preparation, mouse tumor treatment, and so on) and the scientists must keep careful track of conditions. It would be exceedingly difficult to blind such studies.

Reporting for specific materials, systems and methods

We require information from authors about some types of materials, experimental systems and methods used in many studies. Here, indicate whether each material, system or method listed is relevant to your study. If you are not sure if a list item applies to your research, read the appropriate section before selecting a response.

Materials & experimental systems

n/a	Involved in the study
☐	☒ Antibodies
☐	☒ Eukaryotic cell lines
☒	☐ Palaeontology and archaeology
☐	☒ Animals and other organisms
☒	☐ Human research participants
☒	☐ Clinical data
☒	☐ Dual use research of concern

Methods

n/a	Involved in the study
☒	☐ ChIP-seq
☐	☒ Flow cytometry
☒	☐ MRI-based neuroimaging

Antibodies

Antibodies used: See Supplementary Table 2 'Antibody information' in Supporting Information.

Validation: All antibodies were verified by the supplier and each lot has been quality tested. All validation statements can be found on the respective antibody website:
1.Anti-mouse CD11c (FITC): https://www.biolegend.com/en-us/products/fitc-anti-mouse-cd11c-antibody-1815
2.Anti-mouse CD11c (APC): https://www.biolegend.com/en-us/products/apc-anti-mouse-cd11c-antibody-1813
3. Anti-mouse CD86 (PE): https://www.thermofisher.com/cn/zh/antibody/product/CD86-B7-2-Monoclonal-Antibody-GL1-PE-eBioscience/12-0862-83
4. Anti-mouse CD80 (PE): https://www.biolegend.com/en-us/products/pe-anti-mouse-cd80-antibody-43
5. Anti-mouse CD80 (PE/Cy7): https://www.biolegend.com/en-us/products/pe-cyanine7-anti-mouse-cd80-antibody-9320
6. Anti-mouse MHC-II (PE): https://www.biolegend.com/en-us/search-results/pe-anti-mouse-i-a-i-e-antibody-367
7. Anti-mouse SIINFEKL-H2Kb (APC): https://www.biolegend.com/en-us/products/apc-anti-mouse-h-2kb-bound-to-siinfekl-antibody-7882
8. Anti-mouse IFN-γ (PE): https://www.biolegend.com/en-us/products/pe-anti-mouse-ifn-gamma-antibody-997
9. Anti-mouse CD8a (PerCP/Cy5.5): https://www.biolegend.com/en-us/products/percp-cyanine5-5-anti-mouse-cd8a-antibody-4255
10. Anti-mouse CD4 (APC/Cy7): https://www.biolegend.com/en-us/products/apc-cyanine7-anti-mouse-cd4-antibody-1964
11. Anti-mouse CD3e (APC): https://www.biolegend.com/en-us/products/apc-anti-mouse-cd3epsilon-antibody-21
12. Anti-mouse CD8a (PerCP): https://www.biolegend.com/en-us/products/percp-anti-mouse-cd8a-antibody-4256
13. Anti-mouse/human CD44 (PE): https://www.biolegend.com/en-us/products/pe-anti-mouse-human-cd44-antibody-2206

14. Anti-mouse CD45 (Alexa Fluor 488): https://www.biolegend.com/en-us/search-results/alexa-fluor-488-anti-mouse-cd45-antibody-3100
15. Anti-mouse CD62L (APC): https://www.biolegend.com/en-us/products/apc-anti-mouse-cd62l-antibody-381
16. Anti-mouse Foxp3 (PE): https://www.biolegend.com/en-us/products/pe-anti-mouse-foxp3-antibody-4660
17. Anti-mouse CD8a: https://bxcell.com/product/m-cd8a-2/
18. Mouse IgG-UNLB: https://www.southernbiotech.com/?catno=0107-01&type=Polyclonal#&panel1-1&panel2-1
19. Goat anti-mouse IgG1 (HRP): https://www.abcam.com/goat-mouse-igg1-hrp-ab97240.html
20. Goat anti-mouse IgG2a (HRP): https://www.abcam.com/goat-mouse-igg2a-heavy-chain-hrp-ab97245.html
21. Anti-mouse PD-1: https://bxcell.com/product/m-cd279/
22. Anti-mouse CTLA4: https://bxcell.com/product/m-ctla4/
23. Anti-mouse CD16/32: https://www.biolegend.com/en-us/search-results/purified-anti-mouse-cd16-32-antibody-190
24. Anti-mouse-CD3e -PE: https://www.biolegend.com/en-us/products/pe-anti-mouse-cd3-antibody-47
25. Anti-mouse-CD40-PE: https://www.biolegend.com/en-us/products/pe-anti-mouse-cd3-antibody-47
26. Anti-mouse-CD8a-APC: https://www.biolegend.com/en-us/products/apc-anti-mouse-cd8a-antibody-150
27. Anti-mouse-CD3 -FITC: https://www.biolegend.com/en-us/products/fitc-anti-mouse-cd3epsilon-antibody-23
28. Anti-mouse-IFN-γ-PE: https://www.thermofisher.com/cn/zh/antibody/product/IFN-gamma-Antibody-clone-XMG1-2-Monoclonal/17-7311-82
29. Anti-mouse-CD8-PE: https://www.bdbiosciences.com/eu/reagents/research/antibodies-buffers/immunology-reagents/anti-mouse-antibodies/cell-surface-antigens/pe-rat-anti-mouse-cd8a-53-67/p/553033

Eukaryotic cell lines

Policy information about cell lines

Cell line source(s)	Mouse 4T1, B16F10 and CT26 cells were obtained from obtained from the Cell Bank, Shanghai Institutes for Biological Sciences, Chinese Academy of Sciences. HEK-DualTM Null (NF/IL8) cells and HEK-DualTM mTLR4 (NF/IL8) were obtained from Invivogen. B16-OVA cells were gifted from Prof. Haiyan Liu (Soochow University). DC2.4 cells were gifted from Prof. Chao Wang (Soochow University). Primary bone marrow-derived dendritic cell (priBMDC) cells were prepared and cultured by following a standard protocol as previously described (Reference 38)
Authentication	Identity of the cell lines were frequently checked by their morphological features but have not been authenticated by the short tandem repeat (STR) profiling.
Mycoplasma contamination	All cell lines were tested for mycoplasma contamination. No mycoplasma contamination was found.
Commonly misidentified lines (See ICLAC register)	No commonly misidentified cell lines are used in this study.

Animals and other organisms

Policy information about studies involving animals; ARRIVE guidelines recommended for reporting animal research

Laboratory animals	Female C57BL/6 mice (6-8 weeks) and female BALB/c mice (6-8 weeks) were purchased from Nanjing Pengsheng Biological Technology Co., Ltd. Female OT-I transgenic mice (6-8 weeks) were a kind gift from Prof. Xuefeng Wang, Soochow University (China). Female gene knockout Tlr4-/- mice (6-8 weeks) were purchased from GemPharmatech Co., Ltd. Mice were housed in groups of 5 mice per individually ventilated cage in a 12-h light–dark cycle (8:00–20:00 light; 20:00–8:00 dark), with constant room temperature (21±1°C) and relative humidity (40-70%). All mice had access to food and water ad libitum.
Wild animals	The study did not involve wild animals.
Field-collected samples	The study did not involve samples collected from the field.
Ethics oversight	The experimental protocols were approved by the Institutional Animal Care and Use Committee (IACUC) of the Animal Experiment Center of Soochow University (Suzhou, China). All animal experimental procedures were performed in accordance with the Regulations for the Administration of Affairs Concerning Experimental Animals approved by the State Council of the People's Republic of China.

Note that full information on the approval of the study protocol must also be provided in the manuscript.

Flow Cytometry

Plots

Confirm that:

☒ The axis labels state the marker and fluorochrome used (e.g. CD4-FITC).

☒ The axis scales are clearly visible. Include numbers along axes only for bottom left plot of group (a 'group' is an analysis of identical markers).

☒ All plots are contour plots with outliers or pseudocolor plots.

☒ A numerical value for number of cells or percentage (with statistics) is provided.

Methodology

Sample preparation	The inguinal lymph nodes were surgically removed from the vaccinated mice, and then processed through mechanical disruption before digestion for 30 min at 37 °C in RPMI-1640 (10% heat-inactivated FBS and 1% PS) containing 1.5mg/mL collagenase IV(Sigma), 1.5mg/mL collagenase I (Sigma), 1.5 mg/mL hyaluronidase (Sigma), and 0.2 mg/mL DNase I (Sigma). The samples were then passed through 200-mesh nylon mesh filters to obtain single-cell suspensions. We isolated the splenocytes by mincing the spleen from the immunized mice through 200-mesh cell strainers and red blood cells (RBCs) were then lysed using RBC lysis buffer. For tissue sample, the tissue was first mechanically disrupted from mice and divided into small pieces and homogenized in coldstaining buffer to form single cell suspensions in the presence of digestive enzyme. For all samples, cells were first stained with antibodies against surface antigens. In some experiments, cells were subsequently fixed, permeablized and stained for intracellular antigens.
Instrument	BD, FACS Verse and BD AccuritTM C6 Plus
Software	FlowJo software package (version 10.4)
Cell population abundance	No sorting was performed.
Gating strategy	Gating strategies are referred to those described in the website (https://www.bio-rad-antibodies.com/blog/a-guide-to-gating-in-flow-cytometry.html). In general, cells were first gated on FSC/SSC. Singlet cells were gated using FSC-H and FSC-A. Surface and intracellular antigen gating was performed on the singlet cell population. The cell populations within the gate were further analysised based on expression of markers. Single positive straining were uesd to determing the "true" positive. Gating was then based on positive level (after proper compensation). The detailed gating strategy could be found in supporting information.

☒ Tick this box to confirm that a figure exemplifying the gating strategy is provided in the Supplementary Information.